ACADEMIA MILITAR
MILITARY ACADEMY

universidade de aveiro
theoria poiesis praxis

# Calibration Techniques for a New Space Radar Cassegrain Antenna Pointing System

**Nilton José Gomes Rainho Bárbara**

Thesis to obtain the Master of Science Degree in

## Military Electrical and Computer Engineering, specialty Signals

Supervisors: Prof. José Miguel da Silva Bergano (UA)
Prof. José Silvestre Serra da Silva (AM)

**October 2023**

# Acknowledgments

Even tho words do not sufficiently capture the depth of gratitude and love I feel towards my mother, the bedrock of my life, I still wish to thank her. You have instilled in me the values of diligence and tenacity. Your sacrifices and relentless faith in me have lit the path I carved throughout my academic journey. This milestone, although attributed to me, is an undeniable testament to your love and dedication.

In this moment, with the culmination of my thesis and the near end of the course, a profound sense of relief, accomplishment, and joy envelops me. This journey has been both lengthy and challenging. However, each step became lighter thanks to the support and belief of those who surround me.

To my Stephi, your love, patience, and understanding have been my anchor throughout this journey. Your daily encouragement and unwavering belief in me, even during the toughest moments, have been my strongest driving force. I am profoundly grateful for every sacrifice you've made, every word of encouragement you've whispered, and the countless times you've celebrated my smallest victories as if they were monumental.

To my esteemed supervisors, Professor José Silvestre Serra da Silva and Professor José Miguel da Silva Bergano, your guidance, expertise, and patience have been nothing short of instrumental. Through you, I've discovered the virtues of resilience, commitment, and the refined art of discernment. Special thanks to Professor José Silvestre Serra da Silva whose expertise and guidance have been invaluable. Your patience, wisdom, and encouragement have been pillars upon which this work stands.

A heartfelt gratitude goes out to my comrades-in-arms and colleagues. Our mutual challenges, shared experiences, and continued support for one another have forged bonds that transcend mere academics. The camaraderie we fostered during late-night discussions and shared victories will forever be cherished.

Deep thanks to the entire staff, personnel and members of the Military Academy for providing me with the conditions needed to finish this thesis and for fostering an environment conducive to exploration and growth.

A special note of gratitude to the members of Banda de Música do Círculo de Cultura Musical Bombarralense. Your support, passion, and the harmonious moments we've shared have been a source of inspiration and relief amidst the rigorous academic pursuits.

Lastly, my deepest thanks go out to my father, he shaped me into who I am today and despite the fact that he is no longer between us I know that he would be proud. This thesis is not only mine but his as well.

# Resumo

Esta tese de mestrado investiga a possibilidade de adequar o sistema de radiotelescópio localizado em Pampilhosa da Serra para integração nos Sistemas de Defesa de Mísseis Balísticos (SDMB). No cerne deste estudo está uma simulação avançada desenvolvida em MATLAB, meticulosamente desenvolvida para capturar a complexidade inerente a trajetórias de mísseis ballisticos e os desafios em rastreá-los usando sistemas de radar. Através de uma série de cenários, a tese de mestrado explorou o desempenho do Filtro de Kalman Estendido (FKE) no rastreamento de mísseis. As Métricas implementadas para avaliar o desempenho e para avaliar a precisão do rastreamento incluem a Raiz do Erro Quadrático Médio (REQM), o Erro Médio Absoluto (EMA) e o Erro Normalizado de Estimação ao Quadrado (ENEE). É de salientar que, em configurações otimizadas de radar, os valores de REQM atingiram valores tão baixos quanto 41 metros, EMA reduziu para 37 metros e ENEE melhorou significativamente para cerca de 1.5. Estas métricas sublinham o profundo impacto das especificações do radar na precisão do rastreamento e sugerem a potencial eficácia do sistema de radar de Pampilhosa da Serra em aplicações SDMB quando configurado adequadamente.

# Palavras Chave

Sistemas de Defesa de Mísseis Balísticos, Sistema de Radar, Filtro de Kalman Estendido, Simulação MATLAB, Precisão de Rastreamento, REQM, EMA, ENEE.

# Abstract

This master thesis investigates the suitability of the radar system located in Pampilhosa da Serra for integration into Ballistic Missile Defense Systems (BMDS). At the core of this study is an advanced simulation developed in MATLAB, meticulously designed to capture the intricacies of missile trajectories and the challenges in tracking them using radar systems. Through a series of simulated scenarios, the study explored the performance of the Extended Kalman Filter (EKF) in tracking missiles. Key performance metrics, including the Root Mean Square Error (RMSE), Mean Absolute Error (MAE), and Normalized Estimation Error Squared (NEES), were used to assess the tracking accuracy. Notably, in optimized radar configurations, RMSE values dropped to as low as 41 meters, MAE reduced to 37 meters, and NEES significantly improved to around 1.5. These metrics underscore the profound impact of radar specifications on tracking precision and suggest the potential efficacy of the Pampilhosa da Serra radar system in BMDS applications when appropriately configured.

# Keywords

Ballistic Missile Defense Systems, Radar System, Extended Kalman Filter, MATLAB Simulation, Tracking Accuracy, RMSE, MAE, NEES.

# Contents

# List of Figures

# List of Tables

# Acronyms

**AESA** Active Electronically Scanned Array

**AOA** Angle Of Arrival

**BITE** Built-In-Test Equipment

**BM** Ballistic Missile

**BMD** Ballistic Missile Defense

**BMDS** Ballistic Missile Defense System

**BMTP** Ballistic Missile Trajectory Prediction

**CSTTR** Confirmed Split True Track Rate

**CTTR** Confirmed True Track Rate

**CW** Continuous Wave

**ECCM** Electronic Counter-Countermeasures

**EKF** Extended Kalman Filter

**GFTR** Gap Filling Tracking Radars

**GPs** Gaussian Processes

**HDTV** High-Definition Television

**ICBM** Intercontinental Ballistic Missiles

**IMM** Interacting Multiple Model

**IMM-JPDA** Interacting Multiple Model - Joint Probabilistic Data Association

**IMMUF** Interacting Multiple Model Unscented Filter

**IPDA** Integrated Probabilistic Data Association

**IR** Infrared

**IRBM** Intermediate-Range Ballistic Missiles

**JIPDA** Joint Integrated Probabilistic Data Association

**LD** Lateral Divert

**LSTM** Long Short-Term Memory

**MAE** Mean Absolute Error

**MHT** Multiple Hypothesis Trackers

**MIMO** Multiple-Input Multiple-Output

**MRBM** Medium-Range Ballistic Missiles

**NATO** North Atlantic Treaty Organization

**NEES** Normalized Estimation Error Squared

**NRLMSIS** Naval Research Laboratory Mass Spectrometer And Incoherent Scatter

**PAVE** Precision Acquisition Vehicle Entry Phased Array Warning System.

**PDA** Probabilistic Data Association

**PRF** Pulse Repetition Frequencies

**RCS** Radar Cross Section

**RF** Radio Frequency

**RHCIF** Robust High-Degree Cubature Information Filter

**RMSE** Root Mean Square Error

**SAR** Synthetic Aperture Radar

**SE-JIPDA** Split Event-Joint Integrated Probabilistic Data Association

**SMC** Sequential Monte Carlo

**SRBM** Short-Range Ballistic Missiles

**TBM** Tactical Ballistic Missiles

**UHF** Ultrahigh Frequency

**UKF** Unscented Kalman Filter

# 1

# Introduction

Radio Detection and Ranging, more commonly known as Radar, is the word used to describe systems that employ the transmission of electromagnetic waves directed towards an area of interest. A standard radar employs a transmitter, an antenna, a receiver, and a signal processor. The objective of a radar is to have the wave produced by its antenna hit a potential object of interest, causing the wave to scatter. After receiving part of the scattered wave, apply different signal processing tools and treat the data to detect, locate, track, and recognize various objects.

## 1.1 Motivation

Ballistic Missile (BM) pose a significant threat to national security and international stability. They can be used to deliver nuclear, chemical, or biological weapons. They can travel long distances in a short amount of time, making them difficult to detect and intercept. Their proliferation has increased in recent years, with more countries acquiring or developing their missile capabilities. This increase in potential adversaries with missile capabilities makes it even more critical for countries to have effective defense systems.

The development and deployment of Ballistic Missile Defense System (BMDS) can prevent potential adversaries from using missiles in the first place. A country with a credible defense system may make an adversary think twice about launching a missile attack. These are crucial for the protection of civilians. Missile attacks can have devastating consequences for civilians, and effective defense systems can help to protect them from harm.

As a member of the North Atlantic Treaty Organization (NATO), Portugal is responsible for contributing to the alliance's collective defense. NATO has a missile defense system in place to protect member states, and Portugal has played a role in this system by contributing resources and personnel. Being situated on the Atlantic Ocean, near North Africa and the Middle East, which are regions with potential for conflict and the use of missiles, Portugal must be able to defend itself and its allies against missile attacks.

In 2020, there were reports of a possible missile threat to Lisbon from a group in North Africa. This incident highlights the importance of having a robust missile defense system to protect the country and its citizens.

## 1.2 Problem Definition

Algorithms are essential tools many Ballistic Missile Defense (BMD) systems take advantage of as they process and analyze the data collected by radars. However, several challenges and problems are associated with using algorithms in missile defense.

One problem is that algorithms can be complex and require significant computing power to process the data in real-time. This can make it difficult to quickly and accurately analyze the data, which is critical for effective missile defense. Algorithms can be susceptible to errors or biases, affecting their performance and accuracy. For example, if the data used to train the algorithm is incomplete or inaccurate, the algorithm may produce incorrect results. Additionally, if the algorithm is designed with certain biases or assumptions, it may not accurately reflect the real-world situation. There is also the issue of countermeasures. Adversaries may use various tactics to evade or confuse missile defense systems, such as decoys or chaff (strips of metal that can confuse radar). These countermeasures can make it more difficult for algorithms to detect and track missiles accurately, compromising the defense system's performance.

## 1.3 Objective

This work is focused on the crucial aspect of BMD, specifically the calibration techniques used for radar Cassegrain antenna pointing systems. It aims to gain a deeper understanding of the current methods and identify areas for improvement. The research will assess the limitations and challenges associated with these techniques and aim to develop a new calibration method that addresses these issues and provides greater accuracy and precision. The new method's effectiveness will be tested through simulations and experiments, and practical recommendations will be made for its implementation in future BMD radar systems.

## 1.4 Thesis' Structure

The following master's thesis is divided into a total of 6 chapters:

- **Chapter 1 - Introduction:** This chapter sets the stage, introducing the research's motivation and primary objectives. The significance of the study is highlighted, guiding readers into the heart of the investigation.
- **Chapter 2 - Background** Delving into the foundational concepts, this chapter covers the basics of radar systems and missile trajectories.
- **Chapter 3 - State-of-the-Art** An exploration of the latest advancements and methodologies in missile defense radar systems is presented.
- **Chapter 4 - Methodology** Here, the research methods and simulation approaches used to assess the radar system's effectiveness are detailed.
- **Chapter 5 - Results** This chapter presents the findings from the simulations, offering a clear insight into the radar system's performance under various conditions.
- **Chapter 6 - Conclusions** The final chapter draws conclusions based on the results, discusses potential improvements, and suggests directions for future research.

# 2

# Background

This chapter focuses on the main concepts of Radars and, more specifically, BMD radars. It starts with an overview of Radars, Ballistic Missiles and the trajectory they follow, BMD radars and how they work, and finally, a dive into the current state of the art in BMD radars, including the latest advancements and technological innovations.

Radar, a term originating as an acronym for ”Radio Detection and Ranging”, represents one of the pinnacles of electromagnetic systems designed to discern the presence, location, and, often, the velocity of objects. By transmitting electromagnetic waves, typically in the radio or microwave frequency range, a radar system gauges the characteristics of objects within its surveillance area by monitoring the echoes that result from these waves' interaction with potential targets.

At its core, the fundamental mechanism of radar operation lies in the emission of these waves and the subsequent analysis of the reflected signals or ”echoes” that return from the objects being targeted, which interrupt and scatter the wavefront. When an emitted electromagnetic wave encounters an object, part of the wave's energy is deflected back toward the radar, carrying with it information about the object's properties. The time taken for the emitted wave to travel to the object and then return as a reflected wave provides a direct measure of the distance or range to that object. Moreover, by making use of the Doppler effect (a shift in frequency for moving objects), the radial velocity of a target can be determined, offering insights into its motion.

The utility of radar systems extends far beyond mere object detection. By incorporating complex processing algorithms and techniques, modern radars can distinguish multiple closely spaced objects, filter out irrelevant signals or ”clutter” from sources like terrain or weather, and even classify targets based on their radar cross-section or movement patterns. This feature set has cemented radar’s role as an invaluable tool, not just in military applications for which it was originally developed, but also in civilian applications like air traffic control, maritime navigation, and meteorology.

Within the vast number of radar systems, differentiation is often made based on the radar’s primary function, operational frequency, coverage range, and application domain. For instance, primary radars, relying solely on analyzing returned signals, stand in contrast to secondary radars, which operate based on interrogating transponders fitted to targets. Similarly, while some radars provide broad, omnidirectional coverage by scanning the entire horizon, others focus their energy on a narrow, directional beam to achieve higher resolution or to track specific targets with greater precision. The evolving landscape of radar technology, underpinned by advancements in electronics, signal processing, and materials science, continues to push the boundaries of what is possible, paving the way for radar systems that are more accurate, resilient, and versatile.

## 2.1 Basic Principles of Radar

The operative principles behind radar technology combine concepts from electromagnetism, signal processing, and kinematics to create a coherent system for remote sensing. The foundation of radar lies in the transmission of electromagnetic waves. These waves, once emitted, propagate at the speed of light, $c$, which is approximately $3 \times 10^8\ m/s$ in a vacuum. When these waves encounter an object or target, a fraction of the energy is scattered in all directions, with a part reflected back to the radar.

$$c = \frac{1}{\sqrt{\varepsilon \times \mu}} \tag{2.1}$$

Where $c$ is the speed of light, $\varepsilon$ is the permittivity of the medium (often taken as the permittivity of free space, $\varepsilon_0$, in air) and $\mu$ is the permeability of the medium (often taken as the permeability of free space, $\mu_0$, in air).

One of the primary functions of radar is to determine the distance or range of a detected object. This is achieved by measuring the time, $\Delta$t, taken for the radar signal to travel to the target and return as an echo. Given the propagation speed of the signal is the speed of light, the range $R$ is calculated as [1]:

$$R = \frac{c \times \Delta \mathrm{t}}{2} \tag{2.2}$$

The division by 2 takes into account the round trip of the signal, traveling to the object and then back to the radar.

Moving objects induce a frequency shift in the reflected signal, a consequence of the Doppler effect. For a target moving directly towards or away from the radar with a velocity $v$, the frequency shift Δf is given by:

$$\Delta \mathrm{f} = \frac{2 v f_0}{c} \tag{2.3}$$

Where $f_0$ is the transmitted frequency of the radar. By measuring this frequency shift, the radar can deduce the radial velocity of the target. The direction of an object relative to the radar is determined by the radar's antenna pointing angle, both in azimuth (horizontal plane) and elevation (vertical plane). Directional information is essential for applications like tracking or guidance.

While these principles form the core of radar's remote sensing capability, they are all combined by numerous signal processing techniques to enhance the clarity, accuracy, and reliability of radar measurements. These enhancements are especially critical in environments with interference, clutter, or when the radar is tasked with distinguishing between multiple closely spaced objects.

## 2.2 Key Components of a Radar System

At the structural level, a radar system's performance is the result of its integrated components, such as illustrated in Figure (2.1), each playing a pivotal role in ensuring the successful detection, processing, and representation of the target's or object's information.

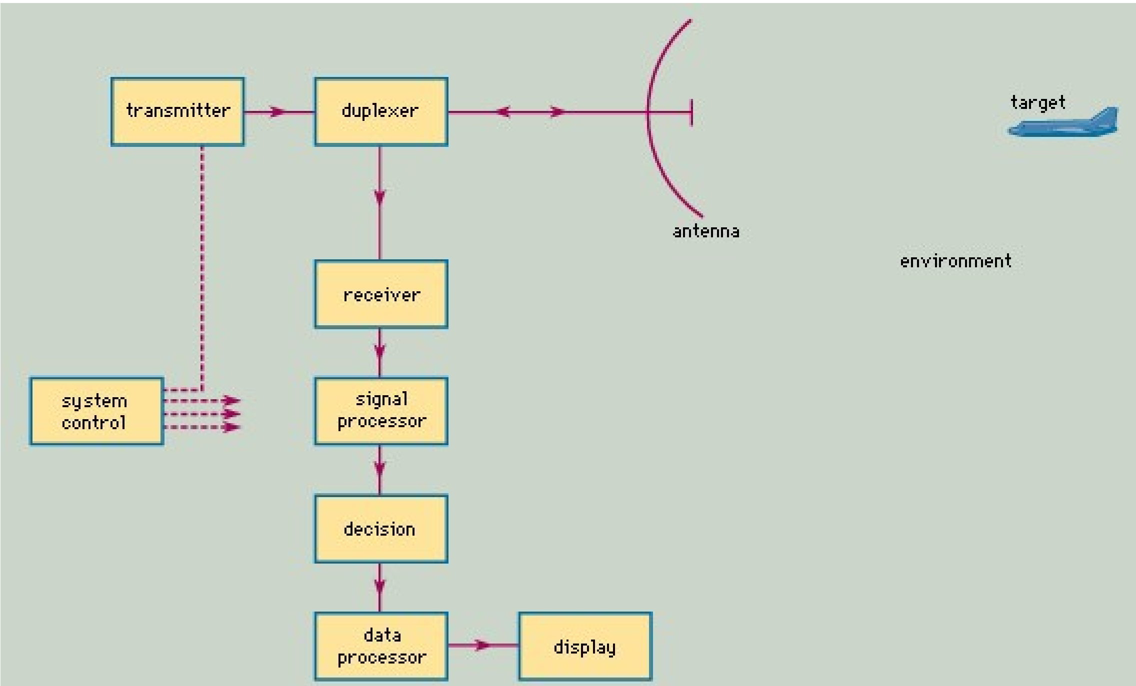


**Figure 2.1:** Basic parts of a radar system
**Source:** https://cdn.britannica.com/80/3680-004-DBB036DC/parts-radar-system.jpg?s=1500x700q=85

**Transmitter:** At the core of the radar operation cycle stands the transmitter, responsible for generating and releasing the high-frequency electromagnetic waves that travel across the environment. These waves are synthesized as short bursts or pulses, and the transmitter's use lies not just in generating them but ensuring their stability and controlled emission. The transmitter's performance influences the radar's overall range and resolution, with higher power generally corresponding to longer detection ranges.

**Antenna:** The antenna serves two distinct roles: as a projector and a catcher. In the first role, it efficiently radiates the electromagnetic waves produced by the transmitter into space. In its second role, it captures the returning echoes, ensuring even weak returns are not missed. The design and orientation of the antenna dictate its directivity and gain, crucial factors in determining how well the radar can focus its energy and receive the reflections from specific directions. In many systems, the antenna rotates or moves to scan vast sections of space, providing extensive surveillance.

**Receiver:** Upon the antenna's capture of reflected signals, they are passed onto the receiver. However, these signals are often weak and may be contaminated with noise or irrelevant information. The receiver's core functions involve amplification of the desired signals, filtering out unwanted noise, and converting these signals into a form suitable for further processing. This delicate balancing ensures that the essential details about the detected object, hidden within the returned echoes, are not lost or overshadowed.

**Duplexer:** Given that the same antenna often serves for both transmission and reception, a mechanism is needed to protect the sensitive receiver components from the potent outgoing pulses of the transmitter. The duplexer acts as a switch, ensuring that the transmitter is connected to the antenna during emission and swiftly shifting the connection to the receiver during the reception phase.

**Signal Processing and Display:** Once the receiver has conditioned the incoming signal, the subsequent step involves extracting meaningful information. Modern radars incorporate advanced signal processing techniques to discern targets from background noise, identify moving objects, and even classify detected entities based on their signature. The culmination of this entire operational cascade finds representation on the radar display. Whether it is the iconic 'blip' on a screen, a colored representation of detected rainfall, or a high-resolution image of a landscape, the display translates raw data into interpretable, actionable insights.

## 2.3 Radar in Missile Tracking

Missile tracking stands as one of the most critical and challenging applications of radar technology. Given the high speeds, dynamic trajectories, and often diminutive sizes of missiles, the demands placed on radar systems in this arena are substantially complex.

Missiles, especially ballistic ones, are fast-moving entities. To maintain a consistent track, radar systems designed for missile tracking require extremely high update rates. This ensures that the missile's position is continuously monitored, providing real-time feedback essential for countermeasures or interception attempts. Even slight errors in tracking can result in significant misses when predicting the missile's future position, especially given the long distances over which interceptions might occur. The radar must therefore offer exceptional accuracy in both range and angle measurements to ensure effective tracking and prediction.

Missiles often deploy evasion techniques or countermeasures, such as chaff or flares, to confuse and decoy radar systems. Advanced signal processing algorithms are vital for distinguishing the missile from such countermeasures, ensuring that the real target is consistently tracked. During the terminal phase of a missile's flight or in environments with varied terrain, ground or sea clutter can pose significant challenges. Radar systems must efficiently differentiate the missile signal from these background reflections, ensuring clarity in tracking.

Given the high-altitude trajectories of many ballistic missiles, tracking radar needs a broad elevation coverage. Simultaneously, considering the vast distances over which such missiles can travel, extended range capabilities are a necessity to provide early detection and prolonged tracking.

Tracking the missile is only one part of a broader defense strategy. The radar system often needs to be integrated seamlessly with missile defense systems to provide data necessary for launching interception missiles. This integration demands high reliability and rapid data transfer rates. Modern warfare often sees the deployment of electronic countermeasures aimed at disrupting or deceiving radar systems. Missile tracking radars need to be resilient to such attempts, ensuring their operability even in contested electronic environments.

## 2.4 Types of Radars

The universe of radar systems, rich in its diversity, spans a variety of types. Each type is meticulously crafted to fulfill specific tasks, optimized based on parameters like range, resolution, target type, and operating environment.

**Continuous Wave (CW) Radars:** CW radars transmit a continuous signal, using the Doppler effect to measure the velocity of moving targets. While they provide excellent velocity measurements, they are not inherently capable of determining the range of the target. Given that the primary requirement of missile tracking is to discern both the position and velocity of a fast-moving target, standalone CW radars may fall behind in comparison to other types of radar. However, in conjunction with other systems or in Doppler filter banks, they can play a good role in missile velocity estimation.

**Pulsed Radars:** Pulsed radars emit energy in pulses and then listen for reflections. By measuring the time it takes for the pulse to return, they can determine the range of the target. The Doppler effect also allows them to measure the velocity. Pulsed radars, especially those with high Pulse Repetition Frequencies (PRF), are often used in missile tracking scenarios. Their ability to provide both range and velocity data, coupled with potential high-resolution capabilities, makes them a staple in defense radar systems.

**Monostatic and Bistatic Radars:** Monostatic radars have their transmitter and receiver co-located, meaning that the same antenna is used as a transmitter and receiver, while bistatic radars have them separated by some distance. Bistatic configurations can reduce the threat of being detected by the target. Both configurations can be used in missile tracking. Bistatic setups, due to their stealthier nature, might be preferred when tracking missiles that have electronic countermeasure capabilities.

**Synthetic Aperture Radar (SAR):** SARs utilize the movement of the radar platform to simulate a large 'virtual' aperture, resulting in high-resolution imaging capabilities. While SARs are predominantly used for ground imaging and reconnaissance, their high-resolution capabilities can be beneficial in post-mission analysis or in the identification of static missile launch sites.

**Phased Array Radars:** These radars have electronically steerable beams, which allow rapid direction changes without physically moving the antenna. This property leads to faster scan rates. Phased array radars are particularly well-suited for missile tracking. Their swift scanning capability ensures that fast-moving missiles remain within the radar's gaze, which is crucial for real-time tracking and interception tasks.

The choice of radar type to use is dictated by a large number of factors, from the nature of the missile threat and the environment to the technological and financial resources at hand.

### 2.4.1 Types of Antennas

**Parabolic Reflector:** The dish or parabolic antenna is one of the most iconic and recognizable types of antennas. An example can be seen in Figure 2.2. It consists of a large parabolic dish that reflects and focuses the radar waves onto a smaller receiver or transmitter element placed at the focal point. Parabolic reflector antennas provide high gain and can be used for long-range applications.

**Figure 2.2:** Parabolic Satellite Communication Antenna
**Source:**https://en.wikipedia.org/wiki/File:Erdfunkstelle$_{Raisting_2}.jpgfile$

**Horn Antenna:** A horn antenna, as can be seen in Figure 2.3, is a flared waveguide that is used to radiate or receive electromagnetic waves. It has a wide aperture at one end and gradually narrows down to a smaller opening. Horn antennas have a wide frequency range and are often used in radar systems that require a broad beamwidth.

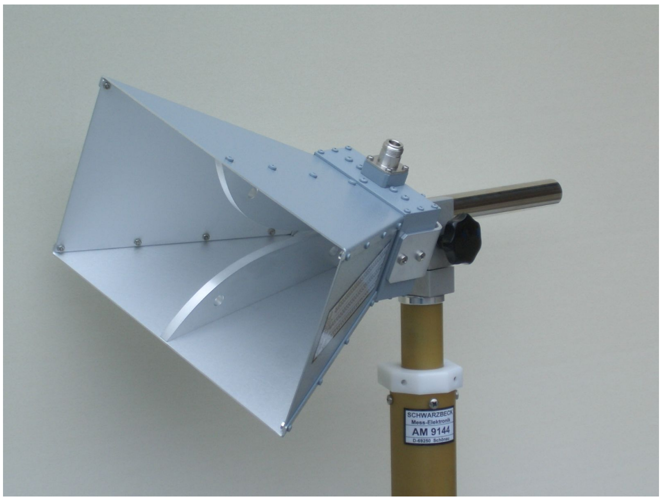


**Figure 2.3:** Broadband Microwave Horn Antenna
**Source:**https://commons.wikimedia.org/wiki/File:Schwarzbeck$_{B}BHA_{9}120_{D}.jpg$

**Phased Array Antenna:** A phased array antenna, as can be seen in Figure 2.4, consists of multiple individual radiating elements, typically in the form of patch antennas or dipole elements arranged in a regular array. By adjusting the phase of the signals fed to each element, the antenna can steer the main beam electronically without physically moving the antenna. Phased array antennas offer rapid beam steering and high agility and have applications in radar systems, communication systems, and military applications.

**Figure 2.4:** Precision Acquisition Vehicle Entry Phased Array Warning System. (PAVE) Phased Array Warning System
**Source:**https://commons.wikimedia.org/wiki/File:PAVE$_{P}AWS_{R}adar_{C}lear_{A}FS_{A}laska.jpg$

**Slot Antenna:** A slot antenna, as can be seen in Figure 2.5, is a type of antenna that uses a slot or aperture in a conducting surface to radiate or receive electromagnetic waves. Slot antennas can be used in radar systems for their low profile and lightweight characteristics. They are often used in applications where size and weight are critical, such as airborne or space-based radar systems.

**Figure 2.5:** Slotted Waveguide Array Antenna
**Source:**https://stocksfox.weebly.com/uploads/1/3/4/1/134189485/545280815.jpg

**Planar Array Antenna:** A planar array antenna, as can be seen in Figure 2.6, consists of a two-dimensional array of radiating elements, typically patch antennas, printed on a planar surface such as a circuit board or a flat panel. Planar array antennas are commonly used in radar systems where a compact and lightweight design is desired, such as in automotive radar or small-scale surveillance radar.

**Figure 2.6:** RLM-ME Radar From 55Zh6MME Radar System
**Source:**https://photos.smugmug.com/Military/ARMY-2023-Static-part-3/i-qc3LxFr/0/b95e0356/X3/Army-2023-Part3-052-X3.jpg

**Yagi-Uda Antenna:** A Yagi-Uda antenna, as can be seen in Figure 2.7, is a directional antenna that consists of a driven element, along with a series of parasitic elements (typically dipoles), and a reflector. It is widely used in radar and communication systems for its high gain and directivity.

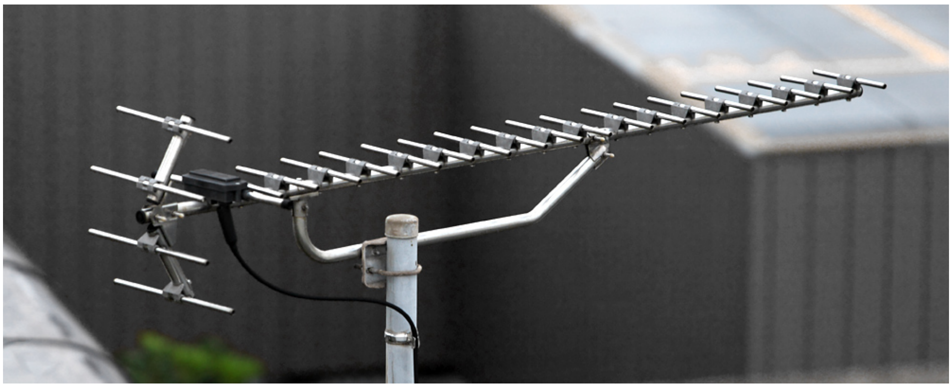

**Figure 2.7:** Yagi Antenna for Ultrahigh Frequency (UHF) High-Definition Television (HDTV) Reception
**Source:**https://commons.wikimedia.org/wiki/File:UHF$_TV_Antenna_01.JPG$

#### 2.4.1.A Parabolic Antennas

**Offset Parabolic Antenna:** The feed is positioned off to the side of the main reflector rather than directly in front of it, as can be seen in Figure 2.8. This arrangement eliminates the feed structure's shadowing effect on the main reflector.

**Cassegrain Antenna:** Uses a hyperbolic secondary reflector (subreflector) placed between the main parabolic reflector and the feed, as can be seen in Figure 2.8. The feed directs energy towards the subreflector, which then reflects it back to the main reflector and out to space.

**Gregorian Antenna:** Similar to the Cassegrain antenna, but uses an ellipsoidal subreflector, as can be seen in Figure 2.8. The feed directs energy forward to the subreflector, which then reflects it back to the main parabolic reflector and outwards.

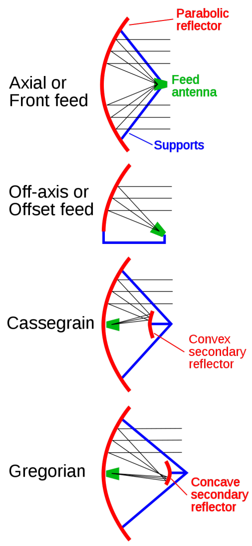


**Figure 2.8:** Most Common Types of Parabolic Antenna Feeds
**Source:**https://commons.wikimedia.org/wiki/File:Parabolic$_antenna_types2.svg$

**Shaped Beam Parabolic Antenna:** The parabolic reflector's shape is modified to produce a non-uniform radiation pattern tailored for a specific application, as can be seen in Figure 2.9.

**Figure 2.9:** Airport Surveillance Radar-9
**Source:**https://commons.wikimedia.org/wiki/File:ASR-9$_{R}adar_{A}ntenna.jpg$

**Dual-Reflector Shaped Beam Antenna:** Combines the principles of shaped beam and dual reflector (like Cassegrain) antennas, as can be seen in Figure 2.10. The main and subreflectors' shapes are tailored to produce a custom radiation pattern.

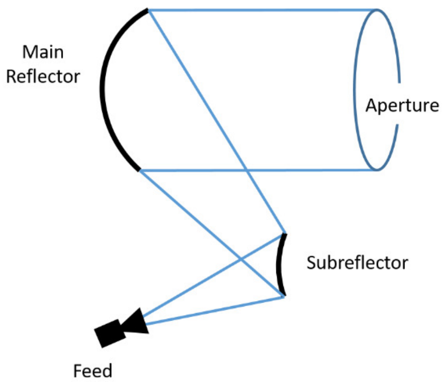


**Figure 2.10:** Offset Dual-Reflector Antenna - Cassegrain Configuration
**Source:**https://www.researchgate.net/publication/341997355/figure/fig1/AS:906737670434823@1593194515867/Offset-dual-reflector-antennas-a-Cassegrain-and-b-Gregorian-configurations.ppm

## 2.5 Radars' Challenges and Limitations

Despite their remarkable capabilities, radar systems are not free of challenges and limitations. Some of these challenges have been an intrinsic part of radar operation since its creation, while others emerge in response to evolving technological and environmental contexts.

The range resolution of a radar, which determines its ability to distinguish between two closely spaced targets along its line of sight, is primarily influenced by the width of the transmitted pulse and the bandwidth of the signal. A narrower pulse or higher bandwidth can improve range resolution, but this often comes at the cost of increased system complexity or reduced energy in each pulse, impacting detection capabilities.

Extraneous reflections, often from terrain, buildings, or the sea surface, also known as clutter, can mask or overshadow signals from desired targets. Similarly, electromagnetic interference, whether accidental or intentional, can affect radar functionality.

While the Doppler effect is exploited to discern moving targets, it introduces a dilemma. In order to detect high-speed targets, a broad Doppler bandwidth is necessary. However, this can reduce the radar's ability to determine slow-moving targets, leading to potential detection blind spots.

In pulsed radar systems, if a target's range exceeds the maximum unambiguous range or its velocity surpasses the maximum unambiguous velocity, it can be misinterpreted as being closer or slower than it truly is. This phenomenon, known as range and Doppler ambiguities, can complicate target identification and tracking.

Modern aircraft and missiles often employ materials and designs intended to reduce radar cross-sections or deflect radar signals away from the source. These stealth technologies challenge radar systems by diminishing the strength of the reflected signal, making detection and tracking more intricate.

The medium through which radar waves travel, primarily the Earth's atmosphere, is not always benign. Different atmospheric layers and conditions can absorb or refract radar waves, influencing their propagation and potentially distorting or attenuating the returned signals.

Particularly for mobile or airborne radar systems, there is a pressing need to balance power, size, and performance. While increased power can augment range and detection capabilities, it also escalates energy consumption and necessitates larger, heavier infrastructure.

## 2.6 Ballistic Missiles

A ballistic missile is a projectile that follows a suborbital trajectory, powered and guided only for a brief initial phase, and then following a free-fall path under the influence of gravity. Such missiles are typically used to deliver one or more warheads to a predetermined target. The trajectory of a ballistic missile can be segmented into three main phases, as seen in Figure 2.11 [1].

### 2.6.1 Boost Phase

This is the initial stage of flight, during which the missile is powered by its rocket engine or engines. The boost phase typically lasts for several minutes, and the missile reaches its maximum altitude and speed during this time. During the boost phase, tracking radars typically use High-Power Radio Frequency (RF) signals and long-range detection capabilities to detect the launch of a missile and track its trajectory as it ascends into the sky.

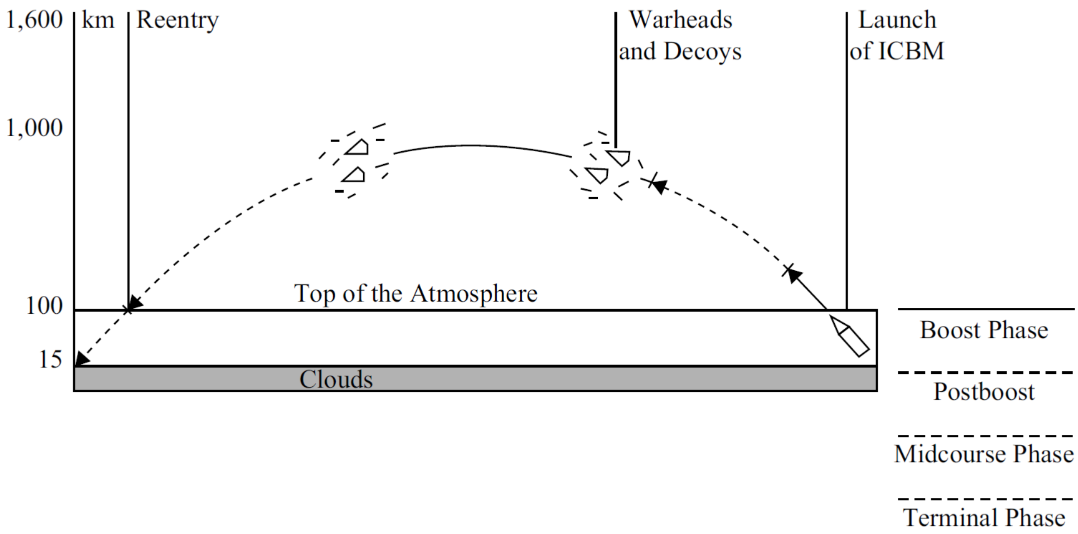


**Figure 2.11:** Ballistic Missile Flight Regimes
**Source:** W. L. Melvin and J. A. Scheer, Principles of modern radar: Radar Applications. SciTech Publishing, 2013.

This may involve using pulse-Doppler processing to measure the Doppler shift of the missile's exhaust plume or other techniques to detect the missile's signature, but it provides early warning to the defense system and allows it to prepare to intercept the missile.

### 2.6.2 Midcourse Phase

This is the next stage of flight, during which the missile is no longer powered and follows a ballistic trajectory under the influence of gravity. The midcourse phase can last several minutes to hours, depending on the missile's range. During the midcourse phase, tracking radars can continue to track the missile as it travels through space. This allows the defense system to predict the missile's possible impact point and to guide interceptor missiles to the correct location. During the midcourse phase, tracking radars can use pulse compression or other techniques to improve their range and resolution, allowing them to track the missile as it travels through space. They may also use Multiple-Input Multiple-Output (MIMO) or Active Electronically Scanned Array (AESA) radar configurations to improve their performance and track multiple objects simultaneously.

### 2.6.3 Terminal Phase

This is the final stage of flight, during which the missile approaches its target and the payload is deployed. The terminal phase typically lasts for only a few seconds, and decoys or other countermeasures may accompany the missile to confuse defenses. During the terminal phase, tracking radars can provide detailed information about the missile's trajectory and help to differentiate between the missile and any decoys or countermeasures that may be deployed. This allows the defense system to make final adjustments to the interceptor's trajectory and ensure that it successfully intercepts the missile. During the terminal phase, tracking radars may use the Angle Of Arrival (AOA) estimation or other techniques to precisely determine the missile's direction and velocity. They may also use clutter rejection algorithms to filter out non-threatening objects and focus on the missile itself.

### 2.6.4 Types of Ballistic Missiles

Ballistic missiles can be categorized based on their range and operational utility:

- Short-Range Ballistic Missiles (SRBM): These missiles have a range of up to 1000 kilometers. Due to their limited range, they are typically used in tactical battlefield scenarios.

- Medium-Range Ballistic Missiles (MRBM): With a range between 1000 to 3000 kilometers, these missiles can target assets in neighboring countries.

- Intermediate-Range Ballistic Missiles (IRBM): Boasting a range of 3000 to 5500 kilometers.

- Intercontinental Ballistic Missiles (ICBM): ICBMs have a range greater than 5500 kilometers and can be used to deliver payloads across continents.

### 2.6.5 Key Components of a Ballistic Missile

Ballistic missiles, while varied in design and purpose, generally contain:

- Rocket Motor/Engine that provides the necessary thrust to propel the missile.

- Guidance System to assist in navigation during the boost phase.

- Warhead acting as the payload, which can be conventional or nuclear.

- Re-entry Vehicle to protect the warhead during the terminal phase, especially from the intense heat generated during atmospheric re-entry.

### 2.6.6 Ballistic Missiles in Modern Warfare

Ballistic missiles have transformed strategic warfare, given their ability to deliver devastating payloads over significant distances in a short time. They act as powerful deterrents and can target key infrastructure, military bases, or cities. The development and proliferation of ballistic missiles, especially with nuclear capabilities, has led to global arms control treaties.

## 2.7 Ballistic Missile Defense Systems

Ballistic Missile Defense (BMD) systems are designed to detect, track, intercept, and destroy incoming ballistic missiles. Due to the different phases of a ballistic missile's trajectory, BMD systems are often designed to counter missiles at specific phases: boost, midcourse, or terminal.

### 2.7.1 Key Components of a BMD System

- Radar Systems used to detect and track the incoming missile.
- Interceptor missiles designed to engage and neutralize the threat.
- Command and Control infrastructures that process data make decisions, and issue commands.
- Communication Systems to ensure seamless communication between different components of the BMD.

## 2.8 Tracking Methods

Tracking radars follow the position of a single target or, in some cases, multiple targets. Compared to a search radar, a tracking radar has a more demanding need for accurate measurements. The working principle behind a tracking radar is to use the error signal to adjust the pointing direction of its antenna, and the difference between the target direction and the reference direction is defined as the angular error. The main tracking methods include lobe switching, conical scanning, and monopulse tracking.

In the lobe switching method, it is required to have two lobes. It is possible with the use of at least one antenna to achieve these two lobes, at the cost of radar performance, and have its beam switch alternately between two positions, having the antenna's boresight and the tracking window follow at the beam's point of overlap. The amplitude measured in both positions will determine the direction in which to turn the antenna. This can be seen in Figure 2.12. A higher voltage means that the target is in the direction of the specific beam. The time taken for the sequencing will represent a significant disadvantage for this method. The radar's Pulse Repetition Frequency (PRF) (nº pulses/second) will determine the time that the receiver will be focused on a particular lobe, and only after the radar has completed the range sweep for a specific PRF will the next lobe be sequenced. Furthermore, the elevation and azimuth error can only be updated once per cycle, adversely affecting the update rate and tracking error. Because lobe switching can be detected, a target can use jamming techniques to break the radar lock.

Conical scanning can be seen as an adapted version of lobe switching. However, for this method, the radar's beam continuously rotates around the antenna's boresight, keeping the target at the center of it. The angle between the axis of rotation and the beam's axis is called the squint angle. Like the previous method, the signal's amplitude will determine in which direction to turn the antenna to maintain the target inside the tracking window, which is shown in Figure 2.13. Due to the actual movement of the beam through space, this method is also easily detected by the target, giving it the possibility of employing jamming techniques to break the radar lock.

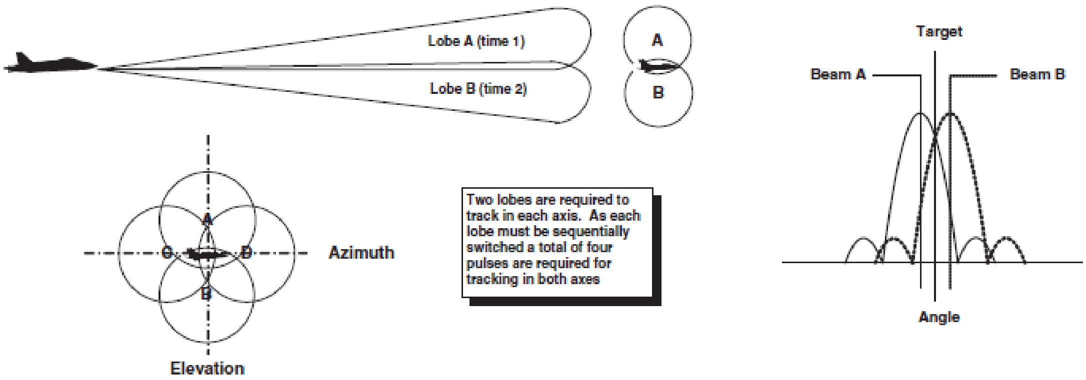


**Figure 2.12:** Lobe Switching - principle of operation
**Source:** https://basicsaboutaerodynamicsandavionics.wordpress.com/2016/08/11/radar-fundamentals-part-ii/

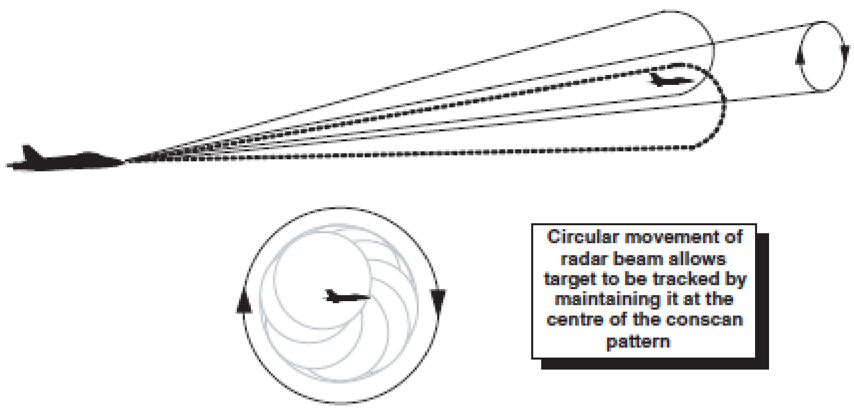


**Figure 2.13:** Conical Scanning - principle of operation
**Source:** https://basicsaboutaerodynamicsandavionics.wordpress.com/2016/08/11/radar-fundamentals-part-ii/

Lastly, the monopluse tracking method, the preferred tracking method of most modern tracking radars, is accurate and hard to deceive. As the name implies, this method's tracking solution can be determined with a single pulse rather than a continuous scan from previous methods. This increases the amount of tracking data for a certain period and consequentially increases its accuracy. This method employs two overlapping antenna patterns, forming a sum pattern and a difference pattern, as shown in Figure 2.14. The sum pattern, used for transmission and reception, provides detection and range measurements of a target. The difference pattern, used only for reception, provides the magnitude of the angular error.

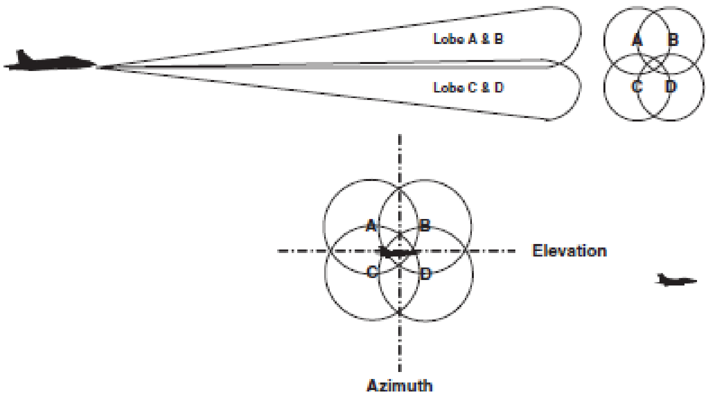


**Figure 2.14:** Monopulse Tracking - principle of operation
**Source:** https://basicsaboutaerodynamicsandavionics.wordpress.com/2016/08/11/radar-fundamentals-part-ii/

## 2.9 Tracking Discrimination

A proper ballistic missile defense system must employ enhanced calibration and alignment techniques and sophisticated algorithms for measurement-to-track data association and track filtering to achieve the required high degrees of measurement-error smoothing, multiple target tracking, and absolute coordinate system registration.

For a missile's trajectory in the exoatmospheric regime, the only forces affecting it are gravitational ones. Track filtering is based on Kalman filters, a set of mathematical equations that provides an efficient computational (recursive) solution of the least-squares method that can achieve a remarkably high degree of smoothing. Depending on the circumstances, a six-state Kalman filter or even a nine-state Kalman filter will optimize tracking performance for a target with more complex aerodynamic forces.

For missiles in a boost or coast regime, the Interacting Multiple Model (IMM) filters can be used to consider booster burnout.

## 2.10 State Estimation Algorithms

Regarding Ballistic Missile defense radar systems, accurate and reliable tracking of incoming missiles is of utmost importance. That is why state estimation algorithms are used to determine the target's position, velocity, and other parameters from radar measurements.

One commonly used method is the Kalman Filter, which can provide accurate estimates despite measurement noise or other uncertainties. The Extended Kalman Filter can be utilized for nonlinear systems, which works by linearizing the system around the current estimate.

Another approach is the Interacting Multiple Model Filter, which can handle dynamic changes in the target's behavior by using multiple models and selecting the most appropriate one. Particle Filters are also a practical option, particularly in complex situations where the system is challenging to model.

These state estimation algorithms play a crucial role in ensuring the performance of BMD radar systems. They can provide early warning of potential threats by providing accurate and reliable tracking of incoming ballistic missiles.

### 2.10.1 Extended Kalman Filter

This work's approach will be focused on the use of Extended Kalman Filters. The filter is potent in several aspects, it supports estimations of past, present, and even future states, and it can do so even when the precise nature of the modeled system is unknown [2].

The state of the target at time $n$ is represented by $x_n$, and the following equations describe the transition of the actual state of the system:

$$\hat{x}_{n+1,n} = F\hat{x}_{n,n} + Gu_n + w_n \tag{2.4}$$

Equation (2.4) is the state extrapolation equation, where $\hat{x}_{n+1,n}$ is a predicted system state vector at a time step $n+1$. Next, we have $\hat{x}_{n,n}$ that represents the system state vector at time step $n$. For $u_n$ we assume a control or input variable. $w_n$ is the process noise. $F$ corresponds to the state transition matrix, and $G$ is the input transition matrix.

$$P_{n+1,n} = FP_{n,n}F^{\mathrm{T}} + Q \tag{2.5}$$

Equation (2.5) is the covariance extrapolation equation, where $P_{n+1,n}$ is the uncertainty of a prediction-covariance matrix for the next state. $P_{n,n}$ represents the uncertainty of an estimate-covariance matrix of the current state, and $Q$ is the process noise matrix.

$$\hat{x}_{n,n} = \hat{x}_{n,n-1} + K_n(z_n - H\hat{x}_{n,n-1}) \tag{2.6}$$

Equation (2.6) corresponds to the state update equation, where $K_n$ represents the Kalman Gain, $z_n$ corresponds to a measurement, and $H$ represents the observation matrix.

$$P_{n,n} = (I - K_n H) P_{n,n-1} (I - K_n H)^T + K_n R_n K_n^T \tag{2.7}$$

Equation (2.7) corresponds to the covariance update equation, where $R_n$ represents the measurement uncertainty, and $I$ is an identity matrix.

$$K_n = P_{n,n-1} H^T \left( H P_{n,n-1} H^T + R_n \right)^{-1} \tag{2.8}$$

Equation (2.8) is the equation used to obtain the Kalman gain.

$$z_n = H x_n + v_n \tag{2.9}$$

$$R_n = E(v_n v_n^T) \tag{2.10}$$

$$Q_n = E(w_n w_n^T) \tag{2.11}$$

$$P_{n,n} = E\left(e_n e_n^T\right) = E((x_n - \hat{x}_{n,n})(x_n - \hat{x}_{n,n})^T) \tag{2.12}$$

Equations (2.9), (2.10), (2.11), and (2.12) can be considered auxiliary equations for measurement, measurement uncertainty, process noise uncertainty, and estimation uncertainty, respectively.

In (2.9), $z_n$ represents the measurement vector, $x_n$ represents the system's actual state, $v_n$ represents a random noise vector, and $H$ is the observation matrix.

In (2.10), $R_n$ represents the covariance matrix of the measurement and $v_n$ the measurement error.

In (2.11), $Q_n$ represents the covariance matrix of the process noise and $w_n$ the process noise.

Finally, in (2.12), $P_{n,n}$ is the covariance matrix of the estimation error, $e_n$ is the estimation error, $x_n$ is the system's actual state and $\hat{x}_{n,n}$ is the estimated system state vector at time step $n$.

$$E(X) = \mu_x \tag{2.13}$$

$E$ denotes the expectation of a variable where $\mu_x$ is the mean of the said random variable.

An extended Kalman filter is the nonlinear version of the Kalman filter [2]. The state transition and observation models do not need to be linear functions of the state but may instead be differentiable functions.

$$x_k = f(x_{k-1}, u_k) + w_k \tag{2.14}$$

$$z_k = h(x_k) + v_k \tag{2.15}$$

Here $w_k$ and $v_k$ are the process and observation noises, which are assumed to be zero mean multivariate Gaussian noises with covariance $Q_k$ and $R_k$, respectively. $u_k$ is the control vector.

The function $f$ computes the predicted state from the previous estimate. Similarly, the function $h$ can be used to compute the predicted measurement from the predicted state. However, $f$ and $h$ cannot be applied to the covariance directly. Instead, a matrix of partial derivatives (the Jacobian) is computed.

At each time step, the Jacobian is evaluated with current predicted states. These matrices can be used in the Kalman filter equations. This process linearizes the nonlinear function around the current estimate.

The following equations can be used to employ the Extended Kalman Filter:

$$\hat{x}_{n,n-1} = f(\hat{x}_{n-1,n-1}, u_n) \tag{2.16}$$

Equation (2.16) represents the predicted state estimate equation.

$$P_{n,n-1} = F_n P_{n-1,n-1} F_n^T + Q_n \tag{2.17}$$

Equation (2.17) represents the predicted covariance estimate equation.

$$\tilde{y}_n = z_n - h(\hat{x}_{n,n-1}) \tag{2.18}$$

Equation (2.18) represents the innovation equation.

$$S_n = H_n P_{n,n-1} H_n^T + R_n \tag{2.19}$$

Equation (2.19) represents the residual covariance equation.

$$K_n = P_{n,n-1} H_n^T S_n^{-1} \tag{2.20}$$

Equation (2.20) represents the near-optimal Kalman gain.

$$\hat{x}_{n,n} = \hat{x}_{n,n-1} + K_n \tilde{y}_n \tag{2.21}$$

Equation (2.21) represents the updated state estimate equation.

$$P_{n,n} = (I - K_n H_n) P_{n,n-1} \tag{2.22}$$

Equation (2.22) represents the updated covariance estimate equation. Lastly, equations (2.23) and (2.24) define the state transition Jacobian matrix and the observation Jacobian matrix.

$$F_n = \left.\frac{\partial f}{\partial x}\right|_{\hat{x}_{n-1,n-1}, u_n} \tag{2.23}$$

$$H_n = \left.\frac{\partial h}{\partial x}\right|_{\hat{x}_{n,n-1}} \tag{2.24}$$

### 2.10.2 Interacting Multiple Model Filter

The IMM filter consists of a set of models, each with its prediction step, measurement update step, and a mixing weight that reflects the confidence in each model[3]. During each iteration, the mixing weights are updated based on the measurement residual, and the state and covariance estimates are updated based on the mixing weights. The final state estimate is obtained by combining the estimates from each model.

One of the key advantages of the IMM filter is its ability to switch between models based on observations. This allows the filter to adapt to changes in the system's dynamics, resulting in a more accurate estimate.

The IMM filter involves a set of equations used to estimate the system's state. The exact form of the equations depends on the specific models used, the measurement model, and the application. However, the basic idea of combining multiple models, updating the mixing weights, and updating the state and covariance estimates remains the same.

Kalman filter tracking errors are prone to increase as a target deviates from the trajectory described by the state transition matrix, making a Kalman filter insufficient for tracking multiple targets.The Interacting Multiple Model (IMM) filters get around these problems by creating multiple state models. Each target is assigned a model defining its state, describing its motion with multiple transition matrices.

This filter is a robust and effective method for estimating the state of a dynamic system based on noisy observations. The idea behind the IMM filter is to combine multiple models, each representing a different possible behavior of the system, to estimate the state, resulting in a more accurate and robust estimate than a single model.

### 2.10.3 Particle Filters

Particle filters, also known as Sequential Monte Carlo (SMC) methods, are a family of algorithms used to estimate a dynamic system's state based on noisy observations[4]. They are commonly used in applications where the state space is highly dimensional, and traditional filters such as Kalman filters may not be suitable.

The basic idea behind particle filters is to represent the probability density function of the state using a set of particles. Each particle represents a possible state of the system, and the set of particles collectively represents the uncertainty in the state. In each iteration, the particles are propagated based on the dynamic model, and the weight of each particle is updated based on the measurement residual. The final state estimate is obtained by resampling the particles, considering the weights.

One of the critical advantages of particle filters is that they can effectively handle nonlinear and non-Gaussian systems. They are also relatively easy to implement, as they do not require a complicated linear algebra solution.

The implementation of particle filters involves algorithms and equations to propagate the particles, update the weights, and resample the particles. The exact form of the equations depends on the specific models used, the measurement model, and the application.

## 2.11 Signal Processing

Tracking radars for ballistic missile defense can employ many different signal-processing techniques. Some examples of these techniques, which have been referred to above, include:

Pulse-Doppler processing, which involves transmitting RF signals in short pulses and then using the Doppler shift of the received echoes to determine the target's velocity.

Pulse compression involves transmitting RF signals in short pulses and then using signal processing techniques to compress the received echoes, allowing the radar to detect objects at greater distances and with greater precision.

Multiple-input multiple-output (MIMO) radar is a configuration that uses multiple transmitters and receivers to improve performance. MIMO radar systems can provide higher resolution and better detection performance than traditional single-antenna radars by using multiple antennae.

Active electronically scanned array (AESA) radar uses an array of transmitters and receivers that can be electronically controlled, allowing the radar to change its beamforming pattern and track multiple objects simultaneously rapidly.

Angle of arrival (AOA) estimation is a technique used to determine the direction of a target relative to the radar. It involves measuring the phase difference of the received signal at different antennae and then using this information to calculate the signal's angle of arrival.

# 3

# State-of-the-Art

Ballistic missile defense radar tracking and estimation algorithms have seen several advancements in recent years. The use of active radar seekers is a crucial component in intercepting incoming ballistic missiles. In [5], Verma discusses the challenges of developing an active radar seeker operating at Ka-band, including receiver and circulator design, fast update rate for homing guidance, and maximizing power aperture product while meeting constraints of the missile platform. The results of the mathematical model of the seeker subsystems and an integrated seeker system show an accurate prediction of the seeker's behavior.

Another recent development in the field [6] is the GAX000 radar by Thales SRA, designed to detect ballistic missiles, air-breathing targets, and space objects. The GAX000 is available in three versions - GA1000, GA3000, and GA5000 - and uses a fully digital 2D AESA antenna with dual polarisation elements. It has search and active tracking functions, automatic track initiation, false alarm regulation, comprehensive Electronic Counter-Countermeasures (ECCM) functions, and extended Built-In-Test Equipment (BITE) for diagnostics and maintenance. Thales' experience developing low-frequency early warning radar, including the GA10 radar and DRTLP demonstrator radar, is also discussed.

A new approach for estimating the trajectory of boost-phase ballistic missiles using a gravity-turn model and line-of-sight measurements from space-borne sensors is discussed in [7]. The proposed high-degree cubature

Huber-based filtering method is designed to be robust to non-Gaussian noise, such as glint noise, commonly present in ballistic missile tracking. The results show this approach to be more accurate and robust than existing methods, such as extended Kalman filtering and cubature Kalman filtering, in the presence of non-Gaussian noise.

In [8], a method for estimating the trajectory of a ballistic missile during the ballistic phase using Infrared (IR) images is presented. The method involves a particle filter algorithm, which generates a set of particles representing possible states of the missile and updates them based on observed IR images and a motion model. The evaluation results show an average position error of fewer than 5 pixels, corresponding to less than 2% of the image size, demonstrating accurate trajectory estimates.

A study [9] discusses a new algorithm for the detection and tracking of split targets, particularly in the context of tracking ballistic missiles during their re-entry phase. This phase is particularly challenging because decoys may be deployed, creating multiple track-lets that the radar must distinguish from the real target. This task becomes even more complicated in the presence of clutter due to the low detection rate.

A new algorithm is proposed in [10] called Split Event-Joint Integrated Probabilistic Data Association (SE-JIPDA), based on the Joint Integrated Probabilistic Data Association (JIPDA) algorithm. The SE-JIPDA algorithm provides a mathematical foundation for split target detection and tracking and includes measures for evaluating the algorithm's performance, such as the Root Mean Square Error (RMSE), Confirmed True Track Rate (CTTR), and Confirmed Split True Track Rate (CSTTR). The article discusses previous work in the field of split target tracking and multi-object tracking, including the use of Probabilistic Data Association (PDA) and Integrated Probabilistic Data Association (IPDA) algorithms, as well as two-step Multiple Hypothesis Trackers (MHT) and joint integrated probabilistic data association (JIPDA) algorithms. These algorithms have been used to address the problem of measurement to track association in multi-target tracking systems and to reduce the computational complexity of multi-target tracking algorithms. It is also noted in [10] that earlier tracking algorithms only considered birth, death, and merge events and did not address the split event as a separate event. The split event is essential in ballistic missile tracking because it can transform the single-object tracking problem into a multi-object tracking problem. The authors cite previous work in the field, including using the Interacting Multiple Model - Joint Probabilistic Data Association (IMM-JPDA) algorithm for split target tracking and using Markov chains to reduce the computational complexity of multi-target tracking algorithms.

In [11] it is discussed the anti-attack procedure of a Ballistic Missile defense System (BMDS) at different operating frequencies at its phased-array radar station. The system's performance is evaluated in terms of Lateral Divert (LD), which is the minimum acceleration required for an interceptor to compensate for prediction error for a successful intercept. The estimation extraction is performed using an Extended Kalman Filter (EKF), and simulation results show better performance at higher frequencies for both tracking and intercepting aspects. The study compares the interception performance at various frequencies for a non-maneuvering re-entry enemy Ballistic Missile. The lateral divert is investigated in terms of a zero-lag terminal guidance system. The essential components of BMDS and related issues in tracking and terminal guidance are also discussed. The results show that frequency selection plays a crucial role in the performance of the BMDS, and higher frequencies lead to improved estimation accuracy and prediction performance.

Traditional methods of estimating trajectories are based on a dynamic model of the missile. However, the approach has limitations when considering the changing dynamics of the missile over its flight phases. A model-free method using Long Short-Term Memory (LSTM) networks is proposed in [12] to overcome these limitations. They generate realistic missile trajectories and radar measurement simulations and use these data to train the LSTM network. The proposed method can accurately estimate ballistic missile trajectories and launch points without considering the missile dynamics and parameters. The study's results suggest that the LSTM network is a promising method for solving the problem of ballistic missile trajectory and launch point estimation.

A paper [13] presents a new algorithm for state estimation of ballistic missiles during the boost stage, called the Robust High-Degree Cubature Information Filter (RHCIF). The algorithm is based on the conventional information filter and improves estimation accuracy and numerical stability by using the fifth-degree cubature rule during the time update stage. The measurement update stage uses the Huber technique to improve robustness to non-Gaussian measurement noise, specifically the glint noise. The RHCIF has been demonstrated to provide improved state estimation performance over extended and high-degree cubature information filters through Monte Carlo simulation and trajectory estimation for ballistic missile experiments. The RHCIF algorithm combines the advantages of the information filter and the high-degree cubature rule with the robustness to non-Gaussian noise from the Huber technique.

In [14], Cooperman presents an Interacting Multiple Model (IMM) approach for tracking Tactical Ballistic Missiles (TBM). The IMM is an established target-tracking method commonly used in air defense systems to reduce lags in tracking highly maneuvering targets. The IMM in this study uses three models, each corresponding to the three phases of TBM trajectory: boost, exo-atmospheric, and endo-atmospheric. The models are implemented as 9-state, 6-state, and 7-state Extended Kalman Filters (EKF), respectively, with the state elements being the position, velocity, and acceleration. The IMM algorithm is designed to fuse contacts from multiple sensors, and the study focuses on two sensors, one defined as local and the other remote. The IMM algorithm uses a linear combination of previous outputs, current measurements, and residuals to update the model probabilities and compute the blended track state and covariance outputs. The paper reports the result from a simulation of a TBM trajectory with measurement noise and demonstrates the effectiveness of the IMM in tracking the TBM.

In another such paper [15], a new filter for tracking a ballistic missile during its boost phase is presented. The filter comprises a novel switching algorithm and a modified Interacting Multiple Model Unscented Filter (IMMUF) with a time-variable Markov transition matrix. The filter can estimate a medium-range ballistic missile model's position, velocity, and unknown parameters. Simulations show that the new filter outperforms previous IMMUFs and can estimate a missile's trajectory and parameters. The filter is robust, requiring no prior knowledge of system parameters or missile maneuver timing. The filter was compared to a modified IMMUF and a standard IMMUF and outperformed both.

A method that combines Gaussian Processes (GPs) and a dynamic equation-based numerical integration method to improve the accuracy of Ballistic Missile Trajectory Prediction (BMTP) during this challenging phase is proposed in [16]. The GP is used to train a prediction error model of the boost-phase trajectory database by capturing the relationship between the numerical integration and the unknown error. The final BMTP combines the dynamic equation-based numerical integration and the GP-based prediction error. Simulation results show that the proposed method effectively improves the accuracy of BMTP during the boost phase and provides reliable uncertainty estimation boundaries. The GP-based error learning scheme provides uncertainty information for the predicted trajectory error, which is crucial for determining the warning range centered on the predicted BM state. The proposed method demonstrates better performance compared to existing methods.

# 4

# Methodology

In this Chapter, it is outlined the methodology proposed for the ballistic missile defense radar simulation, focusing on the implementation of the Extended Kalman Filter algorithm.

The proposed methodology implied the development of a simple simulation environment, expanding on it until arriving at a more advanced simulation that represents a real scenario as close as possible. After said simulation was complete, the implementation of a radar and subsequent radar measurements followed. The Extended Kalman Filter algorithm was implemented into the simulation based on the radar measurements, and from the estimated trajectory, various statistics were analyzed.

## 4.1 Simple Simulation

The simple simulation was designed to allow the evaluation of the EKF's algorithm performance and its ability to track and predict the trajectory of incoming ballistic missiles. In order to make it easier to implement, the simulation was first developed as a simple case scenario where the missile's trajectory was based on its launch speed, $v_0$, and launch angle, $\theta$, using only two dimensions ( $x$ and $y$ ), ignoring atmospheric effects such as drag and other external forces. Considering only the gravitational force exerted by Earth.

### 4.1.1 Ballistic Model Definition

The only important kinematic equations to model the two dimension ballistic trajectory of the missile are the following:

$$x(t) = x_0 + v_{0_x} t + \frac{1}{2} a_x t^2 \tag{4.1}$$

$$y(t) = y_0 + v_{0_y} t + \frac{1}{2} a_y t^2 \tag{4.2}$$

$$v_{0_x} = v_0 \times \cos(\theta) \tag{4.3}$$

$$v_{0_y} = v_0 \times \sin(\theta) \tag{4.4}$$

$$v_x(t) = v_0 \times \cos(\theta) + a_x t \tag{4.5}$$

$$v_y(t) = v_0 \times \sin(\theta) + a_y t \tag{4.6}$$

Assuming that there is only acceleration, $a$, in the vertical axis, $y$, meaning that the velocity in the $x$ axis is constant,

$$a_x = 0 \tag{4.7}$$

$$a_y = -g \tag{4.8}$$

it is possible to modify the previous equations (4.1), (4.2), (4.5), and (4.6) into newer ones:

$$x(t) = x_0 + v_{0_x} t \tag{4.9}$$

$$y(t) = y_0 + v_{0_y} t - \frac{1}{2} g t^2 \tag{4.10}$$

$$v_x(t) = v_{0_x} \tag{4.11}$$

$$v_y(t) = v_0 \times \sin(\theta) - gt \tag{4.12}$$

With these equations implemented into the simulation, defining the entire trajectory of the missile is just a matter of plotting $x(t)$ and $y(t)$ for an arbitrary value of $t$. The next step involved defining the radar to be used.

### 4.1.2 Radar Model Definition

For the radar model definition, a rudimentary radar system providing noisy measurements was implemented in an arbitrary position with coordinates $[x, y]$. The true range and azimuth from the radar to the missile at every time step were computed with the following equations:

$$range_{true}(t) = \sqrt{(x(t) - radar_x)^2 + (y(t) - radar_y)^2} \tag{4.13}$$

$$azimuth_{true}(t) = \arctan 2\left(y(t) - radar_y, x(t) - radar_x\right) \tag{4.14}$$

In equations (4.13) and (4.14), the coordinates of the radar, based on a two-dimensional plane, are given by $[radar_x, radar_y]$, and the function $\arctan 2()$ represents the four-quadrant inverse tangent. The previous two equations assume that the radar gave perfect measurements. In order to add noise to them, it was first defined a value for the measurement noise standard deviation matrix, and that matrix was used together with a random number generator in order to implement Gaussian noise into the measurements.

$$range_{noisy}(t) = range_{true}(t) + deviation_{range} \times randomnumber \tag{4.15}$$

$$azimuth_{noisy}(t) = azimuth_{true}(t) + deviation_{azimuth} \times randomnumber \tag{4.16}$$

Only after defining all these equations was it possible to start implementing the Extended Kalman Filter algorithm.

### 4.1.3 Extended Kalman Filter Implementation

An in-depth revision needed to understand the EKF has already been presented in Chapter 2. The EKF is crucial for navigating through the noise in radar measurements, making it possible to concurrently model the non-linear missile dynamics and estimate its actual position and velocity by considering the radar measurement's stochastic nature. The EKF predicts the missile's future state using a linearized state transition model and then updates the state and error covariance estimates when a new measurement comes in [17]. It consistently works between predicting and correcting the missile's path and speed, striving to bring the predicted path as close to the true path as possible. The EKF was implemented within a loop, iterating over all the positions of the ballistic missile's trajectory, but before entering the loop, the following vectors and matrices were defined:

- Initial State, $X_0 = \begin{bmatrix} x & y & v_x & v_y \end{bmatrix}^T$
- Initial State Covariance, $P$
- Process Noise Covariance, $Q$
- Measurement Noise Covariance, $R$
- Estimated State, $X_{est} = X_0$
- Estimated State Covariance, $P_{est}$

The EKF was then executed in a loop while the missile was flying. For each time step, the state vector was predicted, $X_{pred}$, using the State Transition Matrix, $F$, based on the kinematic equations (4.1) and (4.2) [17].

$$F = \begin{bmatrix} \frac{\partial x(t)}{\partial x_0} & \frac{\partial x(t)}{\partial y_0} & \frac{\partial x(t)}{\partial v_{0_x}} & \frac{\partial x(t)}{\partial v_{0_y}} \\ \frac{\partial y(t)}{\partial x_0} & \frac{\partial y(t)}{\partial y_0} & \frac{\partial y(t)}{\partial v_{0_x}} & \frac{\partial y(t)}{\partial v_{0_y}} \\ \frac{\partial^2 x(t)}{\partial x_0 \partial t} & \frac{\partial^2 x(t)}{\partial y_0 \partial t} & \frac{\partial^2 x(t)}{\partial v_{0_x} \partial t} & \frac{\partial^2 x(t)}{\partial v_{0_y} \partial t} \\ \frac{\partial^2 y(t)}{\partial x_0 \partial t} & \frac{\partial^2 y(t)}{\partial y_0 \partial t} & \frac{\partial^2 y(t)}{\partial v_{0_x} \partial t} & \frac{\partial^2 y(t)}{\partial v_{0_y} \partial t} \end{bmatrix} = \begin{bmatrix} 1 & 0 & t & 0 \\ 0 & 1 & 0 & t \\ 0 & 0 & 1 & 0 \\ 0 & 0 & 0 & 1 \end{bmatrix} \tag{4.17}$$

The matrix $F$ only has four rows and four columns in order to be compatible with the matrix $X_{est}$, which only has four rows. Because of this, the state transition function does not model the trajectory of the missile properly. Equations (4.19) and (4.20) are used in order to correct the previous trajectory estimate, taking acceleration into account and making the prediction more accurate.

$$X_{pred}(t) = F \times X_{est}(t-1); \tag{4.18}$$

$$X_{pred_{v_y}}(t) = X_{pred_{v_y}} - g \times t; \tag{4.19}$$

$$X_{pred_y}(t) = X_{pred_y} - 0.5 \times g \times t^2; \tag{4.20}$$

$$P_{pred}(t) = F \times P_{est} \times F^T + Q; \tag{4.21}$$

The Jacobian, $H_j$, of the measurement function, $h$, is also computed at every step, together with the Kalman gain, $K$, and the new estimations for the state and the covariance associated with it.

$$h = \begin{bmatrix} \sqrt{(X_{pred_x} - radar_x)^2 + (X_{pred_y} - radar_y)^2} \\ \arctan 2(X_{pred_y} - radar_y, X_{pred_x} - radar_x) \end{bmatrix} \tag{4.22}$$

$$H_j = \begin{bmatrix} \frac{X_{pred_x} - radar_x}{h[1]} & \frac{X_{pred_y} - radar_y}{h[1]} & 0 & 0 \\ -\frac{X_{pred_y} - radar_y}{h[1]^2} & \frac{X_{pred_x} - radar_x}{h[1]^2} & 0 & 0 \end{bmatrix} \tag{4.23}$$

$$K = P_{pred} \times \frac{H_j^T}{H_j \times P_{pred} \times H_j^T + R} \tag{4.24}$$

$$X_{est}(t) = X_{pred} + K \times \left( \begin{bmatrix} range_{noisy}(t) \\ azimuth_{noisy}(t) \end{bmatrix} - h \right) \tag{4.25}$$

$$P_{est} = \left( \begin{bmatrix} 1 & 0 & 0 & 0 \\ 0 & 1 & 0 & 0 \\ 0 & 0 & 1 & 0 \\ 0 & 0 & 0 & 1 \end{bmatrix} - K \times H_j \right) \times P_{pred} \tag{4.26}$$

### 4.1.4 RMSE, Mean Absolute Error (MAE) and Normalized Estimation Error Squared (NEES)

To evaluate the performance of the EKF, the RMSE, MAE, and NEES between the true trajectory and the estimated trajectory were computed for both $x$ and $y$ coordinates.

RMSE is a measure of the differences between values predicted by a model and the actual values. It is calculated as the square root of the average squared differences between predicted and observed values, giving more weight to larger errors compared to smaller ones. MAE represents the average of the absolute differences between predicted and actual values, providing a linear penalty for each unit of difference, regardless of the error's direction. NEES is a statistical measure used to assess the performance of an estimator, like an Extended Kalman filter. It measures the squared error between the estimated state and the true state, normalized by the estimator's own uncertainty, and is used to check the consistency of an estimator with respect to its own estimated uncertainty.

$$RMSE = \sqrt{\frac{1}{N}\sum_{i=1}^{N}(y_i - \hat{y}_i)^2} \tag{4.27}$$

$$MAE = \frac{1}{N}\sum_{i=1}^{N}|y_i - \hat{y}_i| \tag{4.28}$$

$$NEES = (x - \hat{x})^T P^{-1} (x - \hat{x}) \tag{4.29}$$

In the previous equations (4.27), (4.28), and (4.29), the variable $y_i$ represents the actual observed value at the ith instance of time, the $\hat{y}_i$ the predicted value at the ith instance of time, $N$ the total number of observations, $x$ the true state of the missile, $\hat{x}$ the estimated state from the EKF and $P$ the estimated state covariance matrix from the estimator.

### 4.1.5 Visualization of Results

A plot illustrating the true missile's trajectory, the estimated trajectory from the EKF, and the radar measurements were displayed in order to better visualize the entire scenario just simulated. The Missile's speed in the $x$ and $y$ directions against time, the missile's overall velocity magnitude against time, $v(t)$, and some key performance indicators of the missile's flight, such as maximum altitude, maximum velocity, and total flight time, are all displayed at the end of the simulation.

$$v(t) = \sqrt{v_x(t)^2 + v_y(t)^2} \tag{4.30}$$

## 4.2 Advanced Simulation

For the more advanced simulation, it was necessary to implement more advanced parameters, but based on the simple simulation, it was only a matter of adding or changing equations and formulas to the base.

### 4.2.1 Initial assumptions

In order to save some work and only focus on the important part of this thesis's main objective, some assumptions were established.

First, the simulation initiates the missile's trajectory analysis post-boost phase, a decision rooted both in simplifying the computational model and adhering to real-world relevancy. The omission of the boost phase helps avoid the complexity of modeling the rapid acceleration and atmospheric transition dynamics present since launch, providing a more computationally tractable framework while retaining pivotal elements of the missile's flight.

Second, the Radar system was hypothetically positioned near the anticipated missile's impact point, an assumption grounded in strategic defense planning, where radars are often placed to safeguard critical infrastructures or densely populated areas. In this scenario, the positioning of radars is crucial to optimize detection probabilities and enhance pre-emptive defensive measures.

### 4.2.2 Ballistic Model Definition

The simulation kicked off by establishing the initial conditions for the missile's trajectory, the same as in the simple simulation. The difference is that for the advanced simulation, a three-dimensional environment was considered instead of a two-dimensional plane, and the effects of atmospheric drag, varying gravity, and the Coriolis effect were implemented.

In this advanced simulation, the missile's trajectory was based on its launch speed, $v_0$, azimuth angle, $\phi$, and elevation angle, $\theta$. It is possible to implement equations (4.1) and (4.2) and add a new equation to represent a $3^{rd}$ dimension:

$$z(t) = z_0 + z_{0y}t + \frac{1}{2}a_z t^2 \tag{4.31}$$

With the previous equations it is possible to represent the missile throughout its entire flight trajectory, assuming that the $xy$ plane represents the ground and the $z$ axis represents the height or altitude of the missile. The next step is defining the equations that describe the missile's velocity during the simulation. For the velocities, some elements were added to equations (4.3) and (4.4) to better describe the movement in a 3D environment:

$$v_{0x} = v_0 \times \cos(\theta) \times \cos(\phi) \tag{4.32}$$

$$v_{0y} = v_0 \times \cos(\theta) \times \sin(\theta) \tag{4.33}$$

$$v_{0z} = v_0 \times \sin(\theta) \tag{4.34}$$

$$v_x(t) = v_{0x} + a_x t \tag{4.35}$$

$$v_y(t) = v_{0y} + a_y t \tag{4.36}$$

$$v_z(t) = v_{0z} + a_z t \tag{4.37}$$

The missile's acceleration during flight is impacted by a few key factors like gravity, air resistance, and the Coriolis effect, the simulation comprehensively integrates these elements, ensuring the trajectory is shaped under realistic physical and environmental constraints.

#### 4.2.2.A Gravitational Acceleration

From the law of universal gravitation, the force on a body acted upon by Earth's gravitational force, $F$, is given by:

$$F = \frac{G \times M_E \times m}{R^2} \tag{4.38}$$

Where $G$ is the gravitational constant, $M_E$ is the mass of Earth, $m$ is the mass of the missile and $R$ is the radius of Earth. Together with Newton's second law:

$$F = mg \tag{4.39}$$

It is possible to see that the acceleration due to gravity at sea level, $g$, is given by:

$$g = \frac{G \times M_E}{R^2} \tag{4.40}$$

And the acceleration due to gravity, $g_a$, at any height, $h$, is given by:

$$g_a = \frac{G \times M_E}{(R+h)^2} \tag{4.41}$$

Combining both equations into one provides the equation for the acceleration due to gravity at any height, only depending on the altitude. It was previously mentioned that the $z$ axis represents altitude, with this in mind it is important to note that the gravitational acceleration will only act on said $z$ axis, specifically, it acts in the negative $z$ direction, pulling the missile downward toward the ground:

$$g_a = g \times \left(\frac{R}{R+h}\right)^2 \tag{4.42}$$

#### 4.2.2.B Drag Acceleration

The drag force, $F_D$, and drag acceleration, $a_d$, were calculated from the drag coefficient, $C_d$, air density, $\rho$, the missile's cross-sectional area, $A$, and the missile's speed, $v$,which then was used to calculate the drag acceleration [18]. The air density values used were obtained from the Naval Research Laboratory Mass Spectrometer And Incoherent Scatter (NRLMSIS), an empirical atmospheric model that extends from the ground to the exobase and describes the average observed behavior of temperature, 8 species densities, and mass density via a parametric analytic formulation.

$$v = \sqrt{v_x^2 + v_y^2 + v_z^2} \tag{4.43}$$

$$F_D = \frac{C_d \times \rho \times A \times v^2}{2} \tag{4.44}$$

$$a_d = -\frac{F_D}{m} \tag{4.45}$$

Using the NRLMSIS 2.0 for air density variations with altitude is crucial. It provides data that enables accurate adjustment of $\rho$ at different altitudes, influencing the drag force effectively. The drag acceleration acts in the direction opposite to the missile's velocity vector in accordance with the following equations:

$$a_{d_x} = -\frac{F_D}{m} \times \frac{v_x}{v} \tag{4.46}$$

$$a_{d_y} = -\frac{F_D}{m} \times \frac{v_y}{v} \tag{4.47}$$

$$a_{d_z} = -\frac{F_D}{m} \times \frac{v_z}{v} \tag{4.48}$$

#### 4.2.2.C Coriolis Acceleration

The fact that Earth is rotating affects the missile's path. This involves the missile's velocity and Earth's angular velocity in the calculations [19], [20] [21]. Starting with the Coriolis force, $F_c$:

$$F_c = 2m\left(\vec{\mathbf{v}} \times \vec{\omega}\right) \tag{4.49}$$

where $m$ is the missile's mass, $\vec{\mathbf{v}}$ the missile's velocity vector $\begin{bmatrix} v_x & v_y & v_z \end{bmatrix}$, $\vec{\omega}$ the Earth's angular velocity vector (assuming a northward-pointing axis of rotation) $\begin{bmatrix} 0, & \omega\cos\left(latitude\right), & \omega\sin\left(latitude\right)\end{bmatrix}$, and $\times$ denoting the cross product between the two vectors. From equation (4.49) it is possible to see that:

$$\vec{\mathbf{a_c}} = \frac{F_c}{m} = 2\left(\vec{\mathbf{v}} \times \vec{\omega}\right) \tag{4.50}$$

The cross product operation results in a vector that is perpendicular to both input vectors. In this case, the cross product between the velocity of the missile and the Earth's rotation vector gives the Coriolis acceleration vector in a 3D space, $\vec{\mathbf{a_c}} = \begin{bmatrix} a_{c_x} & a_{c_y} & a_{c_z} \end{bmatrix}$.

#### 4.2.2.D Eötvös Acceleration

The Eötvös effect is an apparent force experienced by an object moving on the Earth's surface due to the combination of the Earth's rotation and the object's own velocity [21].

When an object is moving eastward (with the rotation of the Earth), it is effectively moving faster than the Earth beneath it. This means it experiences a slight reduction in gravitational pull, due to the centrifugal force being greater in the direction of motion. Conversely, when the object is moving westward (against the Earth's rotation), it is moving slower relative to the Earth's rotation, leading to a slight increase in the effective gravitational pull.

The change in gravitational acceleration $\Delta g$ due to the Eötvös effect (when considering eastward-westward motion) is:

$$\Delta g = v_{east} \times \omega \times \cos(latitude) \tag{4.51}$$

where $v$ is the eastward component of the missile's velocity, $\omega$ is the Earth's angular velocity (approximately $7.27 \times 10^{-5}$ rad/s). Assuming that the $x$ axis represents eastward-westward motion of the missile's trajectory, the acceleration component in the vertical direction due to the Eötvös effect is:

$$a_{e_z} = v_x \times \omega \times \cos(latitude) \tag{4.52}$$

While the Eötvös effect is often less pronounced than the Coriolis effect, it is still important in certain applications like the case of ballistic missiles' trajectories.

The simulation adopts a straightforward numerical approach where time is discretized, and the missile's state is updated at each timestep, employing the derived accelerations, and established initial conditions to update velocities and subsequently, the positions. This approach allows for the meticulous plotting of the missile's trajectory in a three-dimensional environment.

Combining all these forces and accelerations it is possible to derive general equations that describe the acceleration, $a$, experienced by the missile at a given point in time:

$$a = \begin{bmatrix} ax_d + a_c(1) \\ ay_d + a_c(2) \\ az_d + a_c(3) - g_a + ae_z \end{bmatrix} \tag{4.53}$$

### 4.2.3 Radar Detection and Tracking

In the advanced simulation, as in the simple simulation, a radar system providing noisy measurements was implemented in an arbitrary position with coordinates [x, y, z]. Radar detection vital to observe the missile's trajectory, was developed by calculating the received power ($P_r$) at every time step.

$$P_r = \frac{P_t \times G^2 \times \lambda^2 \times \sigma}{(4\pi)^3 \times R^4 \times L} \tag{4.54}$$

The advanced simulation employs the radar equation (4.54) for received power, $P_r$, considering the transmitted power, $P_t$, the antenna gain, $G$, the radar wavelength, $\lambda$, the radar cross section, $\sigma$, the range to the target, $R$ and the system's Loss factor, $L$. The loss factor usually combines various factors of the radar system, such as atmospheric absorption, feed losses, mismatch loss, system temperature, etc... The received power is then compared with the noise floor associated with the radar and if said receiver power is greater than the noise floor then it is assumed that the radar makes a measurement. Storing the position of the missile based on range, azimuth, and elevation.

$$range_{true}(t) = \sqrt{(x(t) - radar_x)^2 + (y(t) - radar_y)^2 + (z(t) - radar_z)^2} \tag{4.55}$$

$$azimuth_{true}(t) = \arctan 2\left(y(t) - radar_y, x(t) - radar_x\right) \tag{4.56}$$

$$elevation_{true}(t) = \arcsin\left(\frac{z(t) - radar_z}{range_{true}(t)}\right) \tag{4.57}$$

And like in the simple simulation, adding noise based on a measurement noise standard deviation matrix and a random number generator:

$$range_{noisy}(t) = range_{true}(t) + deviation_{range} \times randomnumber \tag{4.58}$$

$$azimuth_{noisy}(t) = azimuth_{true}(t) + deviation_{azimuth} \times randomnumber \tag{4.59}$$

$$elevation_{noisy}(t) = elevation_{true}(t) + deviation_{elevation} \times randomnumber \tag{4.60}$$

### 4.2.4 The Extended Kalman Filter

The EKF was implemented in the same way as it was implemented in the simple simulation, only difering in the dimensions of the matrices used. Before entering the loop the following vector and matrices were defined:

- Initial State, $X_0 = \begin{bmatrix} x & y & z & v_x & v_y & v_z \end{bmatrix}^T$
- Initial State Covariance, $P$, a $6 \times 6$ matrix
- Process Noise Covariance, $Q$, a $6 \times 6$ matrix
- Measurement Noise Covariance, $R$, a $3 \times 3$ matrix
- Estimated State, $X_{est} = X_0$
- Estimated State Covariance, $P_{est} = P$

- State Transition Matrix, $F = \begin{bmatrix} \frac{\partial x(t)}{\partial x_0} & \frac{\partial x(t)}{\partial y_0} & \frac{\partial x(t)}{\partial z_0} & \frac{\partial x(t)}{\partial v_{0_x}} & \frac{\partial x(t)}{\partial v_{0_y}} & \frac{\partial x(t)}{\partial v_{0_z}} \\ \frac{\partial y(t)}{\partial x_0} & \frac{\partial y(t)}{\partial y_0} & \frac{\partial y(t)}{\partial z_0} & \frac{\partial y(t)}{\partial v_{0_x}} & \frac{\partial y(t)}{\partial v_{0_y}} & \frac{\partial y(t)}{\partial v_{0_z}} \\ \frac{\partial z(t)}{\partial x_0} & \frac{\partial z(t)}{\partial y_0} & \frac{\partial z(t)}{\partial z_0} & \frac{\partial z(t)}{\partial v_{0_x}} & \frac{\partial z(t)}{\partial v_{0_y}} & \frac{\partial z(t)}{\partial v_{0_z}} \\ \frac{\partial^2 x(t)}{\partial x_0 \partial t} & \frac{\partial^2 x(t)}{\partial y_0 \partial t} & \frac{\partial^2 x(t)}{\partial z_0 \partial t} & \frac{\partial^2 x(t)}{\partial v_{0_x} \partial t} & \frac{\partial^2 x(t)}{\partial v_{0_y} \partial t} & \frac{\partial^2 x(t)}{\partial v_{0_z} \partial t} \\ \frac{\partial^2 y(t)}{\partial x_0 \partial t} & \frac{\partial^2 y(t)}{\partial y_0 \partial t} & \frac{\partial^2 y(t)}{\partial z_0 \partial t} & \frac{\partial^2 y(t)}{\partial v_{0_x} \partial t} & \frac{\partial^2 y(t)}{\partial v_{0_y} \partial t} & \frac{\partial^2 y(t)}{\partial v_{0_z} \partial t} \\ \frac{\partial^2 z(t)}{\partial x_0 \partial t} & \frac{\partial^2 z(t)}{\partial y_0 \partial t} & \frac{\partial^2 z(t)}{\partial z_0 \partial t} & \frac{\partial^2 z(t)}{\partial v_{0_x} \partial t} & \frac{\partial^2 z(t)}{\partial v_{0_y} \partial t} & \frac{\partial^2 z(t)}{\partial v_{0_z} \partial t} \end{bmatrix} = \begin{bmatrix} 1 & 0 & 0 & t & 0 & 0 \\ 0 & 1 & 0 & 0 & t & 0 \\ 0 & 0 & 1 & 0 & 0 & t \\ 0 & 0 & 0 & 1 & 0 & 0 \\ 0 & 0 & 0 & 0 & 1 & 0 \\ 0 & 0 & 0 & 0 & 0 & 1 \end{bmatrix}$

For each time step inside the loop, the predicted state, $X_{pred}$, a $6 \times 1$ vector, was calculated following the equations:

$$X_{pred}(t) = F \times X_{est}(t) \tag{4.61}$$

$$X_{pred_x}(t) = X_{pred_x}(t) + 0.5 \times a_x \times t^2 \tag{4.62}$$

$$X_{pred_y}(t) = X_{pred_y}(t) + 0.5 \times a_y \times t^2 \tag{4.63}$$

$$X_{pred_z}(t) = X_{pred_z}(t) + 0.5 \times a_z \times t^2 \tag{4.64}$$

$$X_{pred_{vx}}(t) = X_{pred_{vx}}(t) + a_x t \tag{4.65}$$

$$X_{pred_{vy}}(t) = X_{pred_{vy}}(t) + a_y t \tag{4.66}$$

$$X_{pred_{vz}}(t) = X_{pred_{vz}}(t) + a_z t \tag{4.67}$$

Note that the state transition function does not account for the effect of acceleration into the missile's trajectory, that is why the equations (4.62), (4.63), (4.64), (4.65), (4.66), (4.67) have into them the effect incorporated, in order to properly calculate the $X_{pred}(t)$ vector.

### 4.2.5 Root Mean Square Error (RMSE), Mean Absolute Error (MAE) and Normalized Estimation Error Squared (NEES)

Once the simulation was finished, error metrics like RMSE (4.27), MAE (4.28) and NEES (4.29) were used as a way to quantify the accuracy and reliability of the EKF.

# 5

# Results

In this chapter, it is outlined the conditions in which the simulations were run and the main variables that were being focused on, as well as the results of the simulation. To evaluate the performance of the EKF, various metrics such as Root Mean Square Error, Mean Absolute Error and Normalized Estimation Error Squared were used.

The simulations discussed in previous chapters were developed using the software MATLAB, taking into account values that describe the radio telescope system of Pampilhosa da Serra's astronomical observatory. In order to best study the implementation of the EKF and if it is a worthy algorithm to use in the tracking of ballistic missiles, several simulations were run, diving them into 7 cases of study, each with a specific parameter to study. Across all cases some values remained constant, the simulations were run with 30 constant parameters some of which can be seen in table 5.1.

Where $v_0$ is the launch velocity, $\phi$ the launch azimuth angle, $\theta$ the launch elevation angle, $Lat$ the latitude for the launch position, $Lon$ the longitude for the launch position, $x_{radar}$, $y_{radar}$ and $z_{radar}$ the radar's position, $L$ the radar's Loss factor, $Range_{max}$ the radar's maximum range, $C_d$ the missile's drag coefficient, $m$ the missile's mass and $x$, $y$ and $z$ the missile's start position after boost-phase.

| | |
|---|---|
| $v_0$ | 7000 $m/s$ |
| $\phi$ | 300 deg |
| $\theta$ | 45 deg |
| $Lat$ | 40.105784 deg |
| $Lon$ | 127.066978 deg |
| $x_{radar}$ | $7.5554 \times 10^6$ $m$ |
| $y_{radar}$ | $8.1046 \times 10^6$ $m$ |
| $z_{radar}$ | 0 $m$ |
| $L$ | 1.3 |
| $Range_{max}$ | $1000 \times 10^3$ $m$ |
| $C_d$ | 0.15 |
| $m$ | 362 $kg$ |
| $x$ | 4274030.934 $m$ |
| $y$ | 14512235.624 $m$ |
| $z$ | 170000 $m$ |

**Table 5.1:** Simulation's Constant Values

$$F = \begin{bmatrix} 1 & 0 & 0 & t & 0 & 0 \\ 0 & 1 & 0 & 0 & t & 0 \\ 0 & 0 & 1 & 0 & 0 & t \\ 0 & 0 & 0 & 1 & 0 & 0 \\ 0 & 0 & 0 & 0 & 1 & 0 \\ 0 & 0 & 0 & 0 & 0 & 1 \end{bmatrix} \tag{5.1}$$

$$P = \begin{bmatrix} 4000^2 & 0 & 0 & 0 & 0 & 0 \\ 0 & 4000^2 & 0 & 0 & 0 & 0 \\ 0 & 0 & 4000^2 & 0 & 0 & 0 \\ 0 & 0 & 0 & 50^2 & 0 & 0 \\ 0 & 0 & 0 & 0 & 50^2 & 0 \\ 0 & 0 & 0 & 0 & 0 & 50^2 \end{bmatrix} \tag{5.2}$$

$$R = \begin{bmatrix} 75^2 & 0 & 0 \\ 0 & (\frac{0.2\times\pi}{180})^2 & 0 \\ 0 & 0 & (\frac{0.05\times\pi}{180})^2 \end{bmatrix} \tag{5.3}$$

$$Q = \begin{bmatrix} 100^2 & 0 & 0 & 0 & 0 & 0 \\ 0 & 100^2 & 0 & 0 & 0 & 0 \\ 0 & 0 & 100^2 & 0 & 0 & 0 \\ 0 & 0 & 0 & 10^2 & 0 & 0 \\ 0 & 0 & 0 & 0 & 10^2 & 0 \\ 0 & 0 & 0 & 0 & 0 & 10^2 \end{bmatrix} \tag{5.4}$$

The previous matrices were also kept constant across the seven cases but in order to arrive to those values the EKF had to be tuned across a large number of iterations.

Figure 5.1 shows the simulated missile's trajectory that was studied and to which the EKF was applied. Figure 5.2(a) and 5.2(b) shows the simulated missile's velocity magnitude across time and the missile's speed in each of the 3 dimension, as well, across time. Both the trajectory and the velocity make sense in the context of a

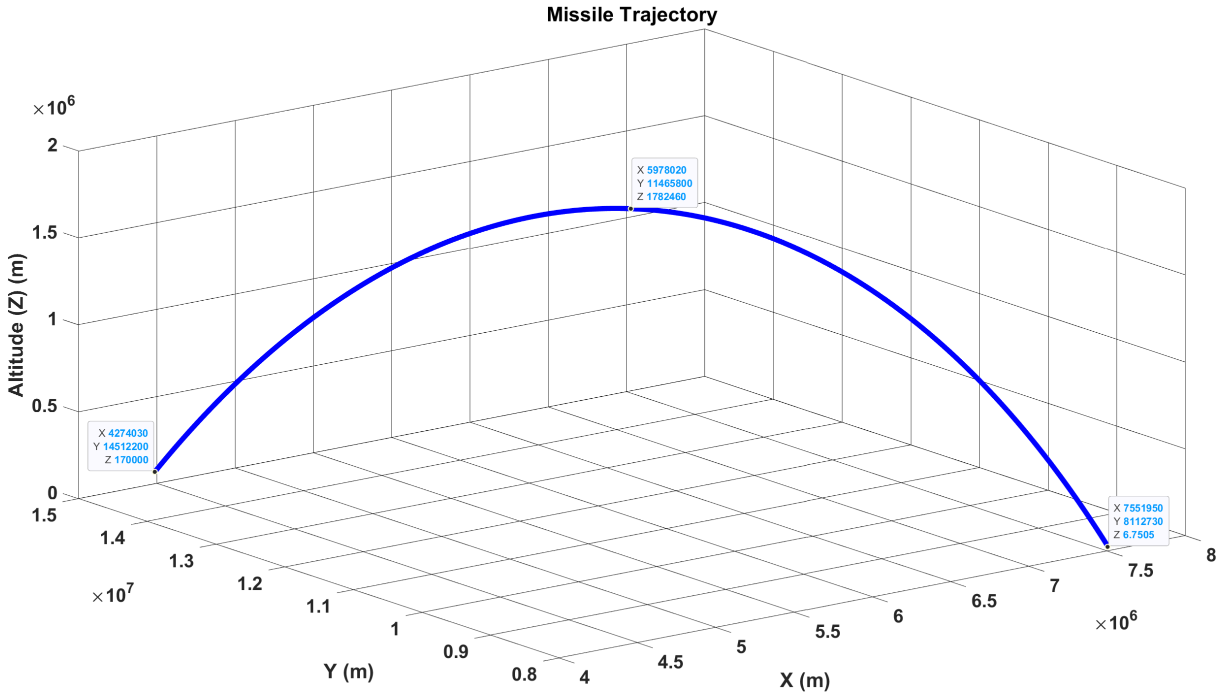


**Figure 5.1:** Ballistic missile's simulated trajectory

ballistic missile that suffers effects from all the previous mentioned in chapter 4, such as drag from re-entering the atmosphere. After simulating the ballistic missile's trajectory and behavior some data can be retrieved from it, table 5.2, together with figures 5.2(a) and 5.2(b) provide some of that data.

| Total Flight Time | Ground Distance travelled | $\text{speed}_{Max}$ | $\text{height}_{Max}$ | Impact Point |
|---|---|---|---|---|
| $1497.1\ s$ | $11.0837 \times 10^6\ m$ | $7137.94\ m/s$ | $17.82 \times 10^5\ m$ | $[7.5, 8.1, 0] \times 10^6\ m$ |

**Table 5.2:** Simulation's Variables

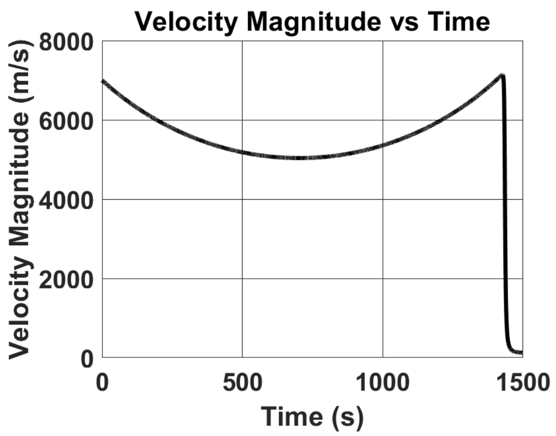


((a)) Velocity Magnitude Vs Time

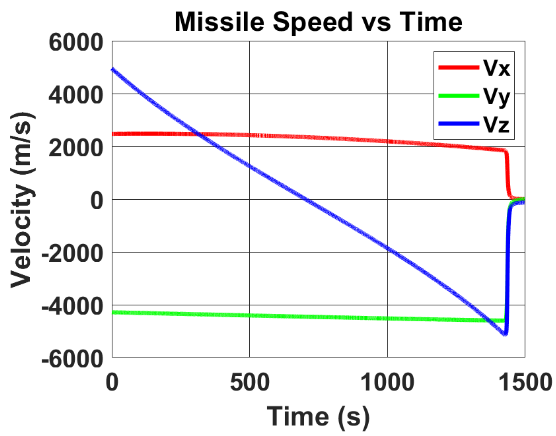


((b)) Missile Speed Vs Time

**Figure 5.2:** Missile's Velocity and Speed

The seven different cases simulated all vary in some aspect with the objective of studying the impact that a radar with different parameters has on the performance of the EKF, the parameters being studied across the seven cases are the minimum range of detection, $Range_{min}$, the power transmitted at peak, $P_{peak}$ and the missile's Radar Cross Section (RCS), $\sigma$.

## 5.1 Cases Studied

For Case A the main objective was to simulate the conditions that are present with the radio telescope system of Pampilhosa da Serra's astronomical observatory in order to see if the station can serve as an appropriate radar to be used in a ballistic missile defense system and at the same time act as a control case. Cases B, C and D serve to see the effect that the missile's RCS can have on the performance of the algorithm. Case E's main objective was to observer the effect that the radar's minimum detection range had on the EKF's performance. Case F's main objective was to observe the effect that the radar's peak power had on the EKF's performance. Case G, the final case's objective was to see how the filter would behave on a best case scenario, with a lower value for the minimum detection range and a higher value of the radar's peak power.

In table 5.3 are the variables for all the seven cases, they had the following values:

| Cases | A | B | C | D | E | F | G |
|---|---|---|---|---|---|---|---|
| $Range_{min}(m)$ | $50\times10^3$ | $50\times10^3$ | $50\times10^3$ | $50\times10^3$ | $50\times10^{-3}$ | $50\times10^3$ | $50\times10^{-3}$ |
| $P_{peak}(W)$ | $5\times10^3$ | $5\times10^3$ | $5\times10^3$ | $5\times10^3$ | $5\times10^3$ | $5\times10^6$ | $5\times10^6$ |
| $\sigma(m^2)$ | 10 | 1 | 100 | 1000 | 10 | 10 | 10 |

**Table 5.3:** Studied Cases' Variables

## 5.2 RMSE vs time

The RMSE provides a quantifiable measure that indicates how closely the EKF predictions come to the true trajectory of the missile, making it a valuable tool for evaluating the robustness of the tracking system. With Figure 5.3 and table 5.4 it is possible to see how the RMSE values vary across all 7 cases.

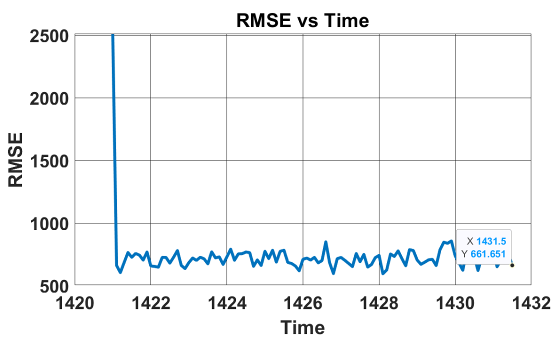


**((a))** Case A

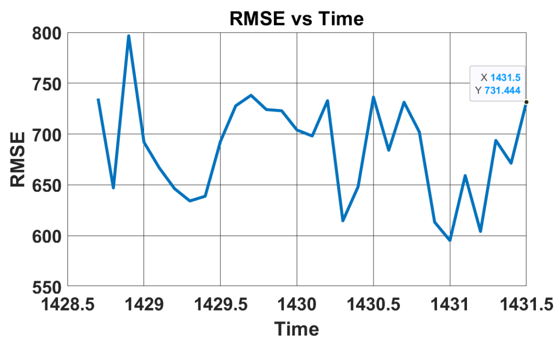


**((b))** Case B

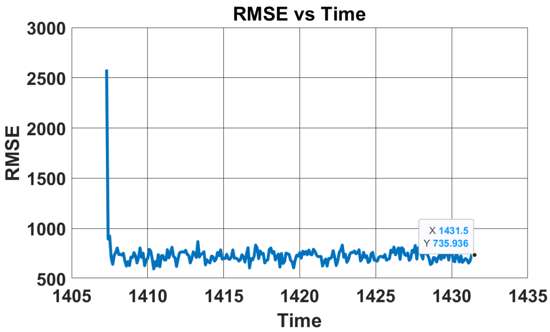


((**c**)) Case C

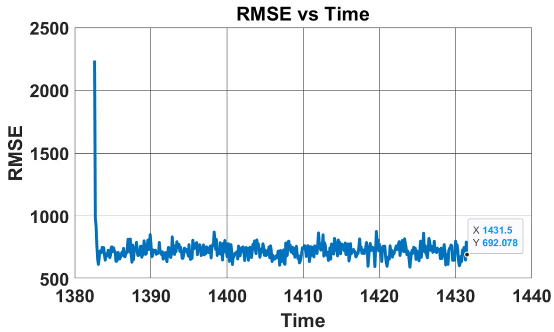


((**d**)) Case D

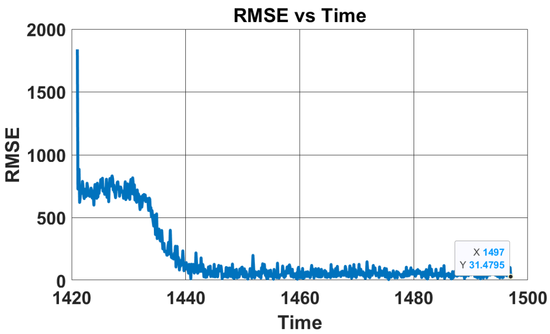


((**e**)) Case E

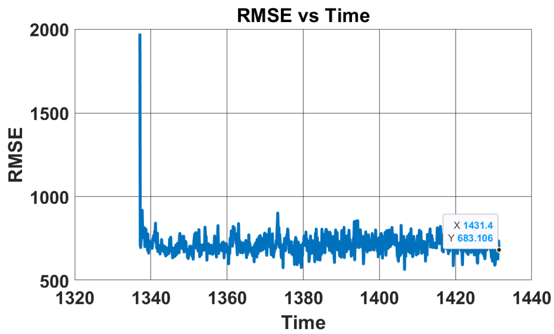


((**f**)) Case F

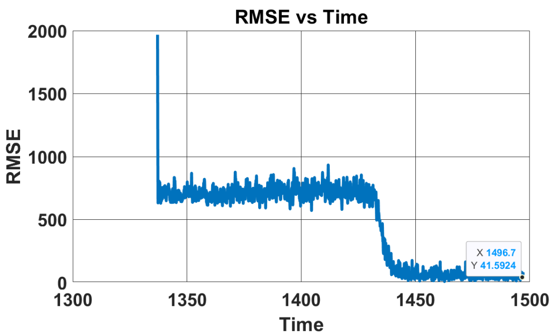


((**g**)) Case G

**Figure 5.3:** Cases' Comparisson - RMSE vs Time

| Cases | A | B | C | D | E | F | G |
|---|---|---|---|---|---|---|---|
| Overall RMSE ($m$) | 732.2431 | 831.4352 | 798.1098 | 736.3096 | 320.2124 | 724.3738 | 563.8943 |
| Tracking window ($s$) | 10.5 | 3.5 | 24.2 | 48.9 | 75.6 | 94.4 | 160 |

**Table 5.4:** Studied Cases' Statistics

Upon observing the RMSE plots across the various cases, it is possible to see that every case exhibits a pronounced spike at the very beginning, the worst one being for case C, the case with an RCS of 100 $m$, with an initial value of RMSE higher than 2500 $m$ and the best one being case B with an initial value under 750 $m$. This spike represents the RMSE value of the EKF's first prediction. Immediately following this spike, the RMSE values experience a sharp decrease. After this decrease, the values settle into a plateau, remain somewhat constant, for a period of time, not showing outrageous fluctuations. The higher values of RMSE from the worst performing cases, A, B, C, D and F, stem from the fact that the minimum detection distance of 50 *km* is not low enough to capture the change in velocity that the missile suffers due to the drag force experienced from re-entering the atmosphere at the 1435 *s* mark. For cases E and G, there is a noticeable drop in RMSE around said mark. After this drop, a new, lower plateau forms where the RMSE stabilizes again, from an average of 750 *m* to an average of 35 *m*. While the absolute values of RMSE might differ from one case to another, the general behavior of the plots remains consistent. All plots exhibit the initial spike, followed by a period of stability, and for cases E and G, the mentioned drop at the 1435 *s* mark. Across all cases the overall value for RMSE is fairly high with an average of 831.4352 *m* for case B, the worst performing case, and an average of 320.2124 *m* for case E. It is worth noting that the data across all cases is uniformly sampled. This consistency ensures that the observed patterns in RMSE values are indicative of the EKF's performance and not a result of variable sampling rates.

## 5.3 MAE vs time

The MAE offers a straightforward measure that quantifies the average magnitude of errors between the EKF predictions and the actual missile trajectory. This metric does not square the errors, which means it gives a linear penalty to all errors irrespective of their size. This makes the MAE especially useful for understanding the real-world impact of prediction errors, as it is less sensitive to large outliers than RMSE. By referring to Figure 5.4 and Table 5.5, one can observe how the MAE values fluctuate across all 7 cases.

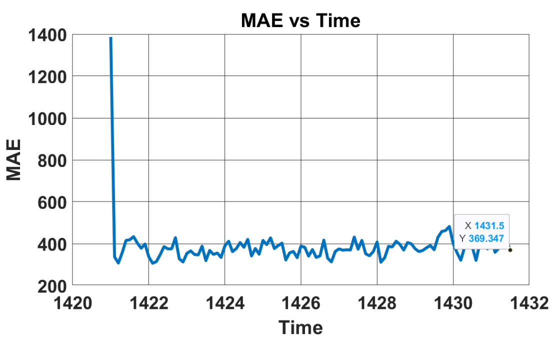


((a)) Case A

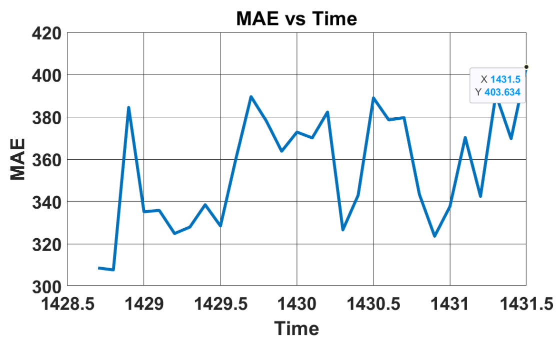


((b)) Case B

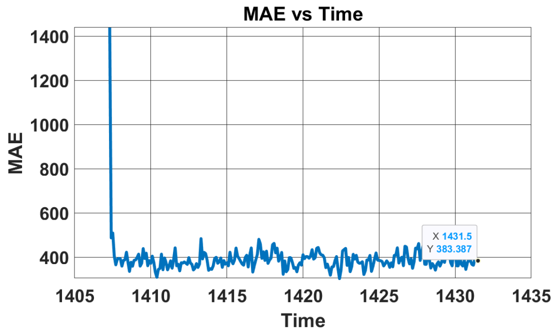


((c)) Case C

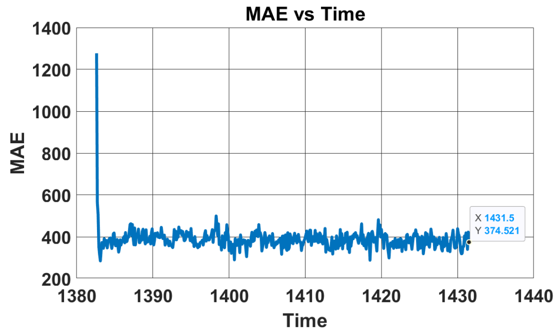


((d)) Case D

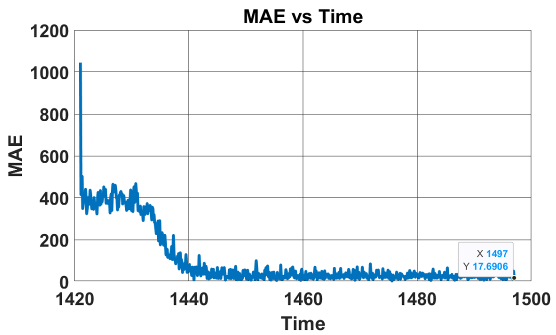


((e)) Case E

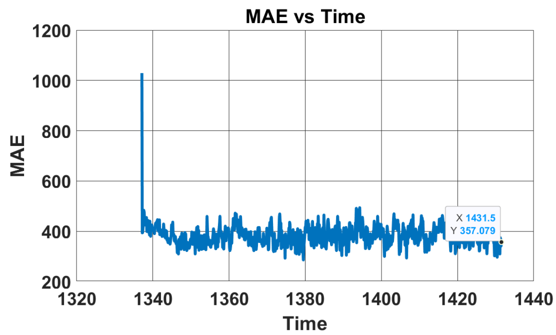


((f)) Case F

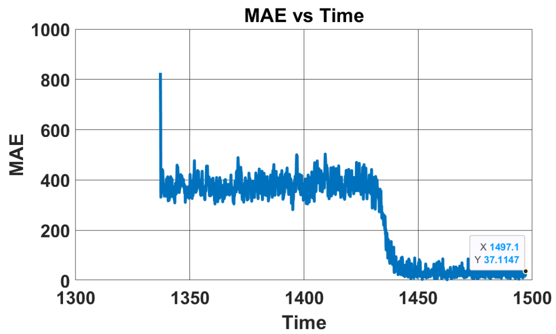


((g)) Case G

**Figure 5.4:** Cases' Comparisson - MAE vs Time

| Cases | A | B | C | D | E | F | G |
|---|---|---|---|---|---|---|---|
| Overall MAE ($m$) | 384.4747 | 415.2629 | 396.4206 | 385.6785 | 98.5622 | 381.4597 | 248.5942 |

**Table 5.4:** Studied Cases' Overall MAE

Upon examining the MAE plots for all cases, it becomes evident that they exhibit a behavior similar to the RMSE plots. Each case starts with a pronounced initial spike, signaling the first prediction error. Following this spike, the MAE values witness a significant decline and stabilize, forming a plateau that remains fairly consistent for a duration. It is important to note that while the trends between RMSE and MAE are similar, the actual values differ. Specifically, the MAE values are generally about half of the corresponding RMSE values. This suggests that while both metrics capture the error in the EKF's predictions, the magnitude of the errors is less severe in MAE, likely due to MAE being less sensitive to large errors.

The higher MAE values in cases A, B, C, D, and F can be attributed to the missile's atmospheric re-entry at the 1435 $s$. The minimum detection distance of 50 $km$ in these cases does not adequately capture the velocity changes the missile undergoes due to atmospheric drag. However, cases E and G, which have a lower detection distance, show a noticeable reduction in MAE values at this time point. Following this drop, the MAE values establish a new plateau, lower than the previous one, highlighting the impact of the missile's re-entry on prediction accuracy.

Across the plots, the average MAE values vary. Case B, while having the smallest initial spike, has the highest average MAE of 415.2629 $m$. Conversely, case E, which captures the missile's atmospheric re-entry, boasts the lowest average MAE of 98.5622 $m$. The consistency in sampling across all cases ensures the observed patterns in the MAE values genuinely represent the EKF's performance.

## 5.4 NEES vs time

The NEES provides a normalized measure to evaluate the accuracy of state estimates compared to their expected accuracy. In essence, it quantifies how well the EKF's internal uncertainty (i.e., its covariance) matches the actual estimation errors. When using the EKF for missile trajectory tracking, it's crucial not just to have accurate estimates, but also for the filter to be aware of its own accuracy. A well-calibrated filter will have NEES values close to the identity, indicating that the estimation errors are in line with the filter's expectations. Referring to Figure 5.5, the variation in NEES values across the 7 cases can be observed.

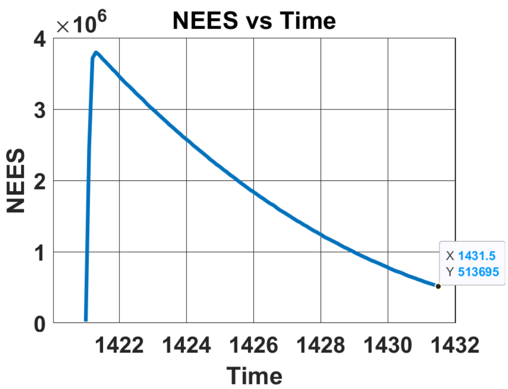

((a)) Case A

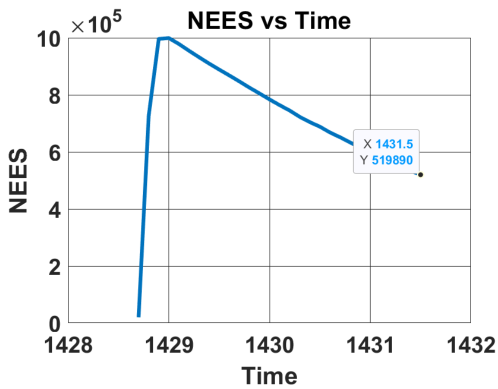

((b)) Case B

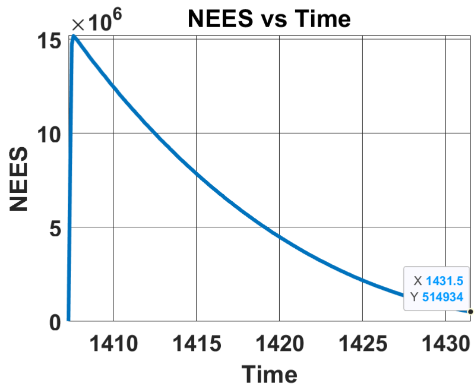


((c)) Case C

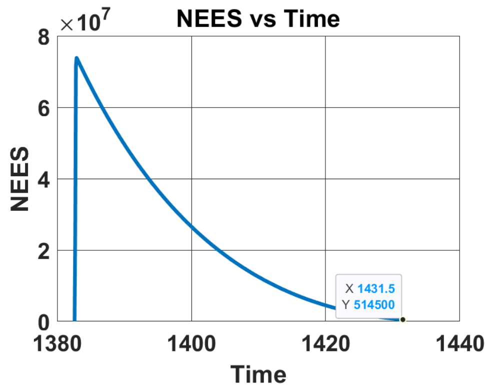


((d)) Case D

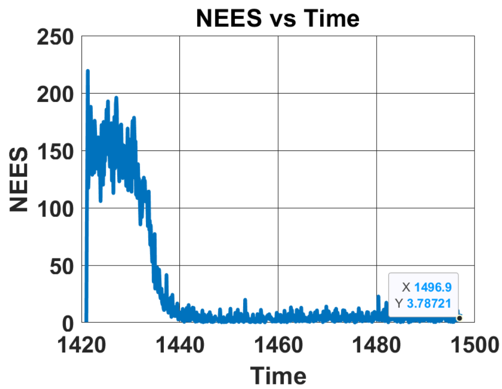


((e)) Case E

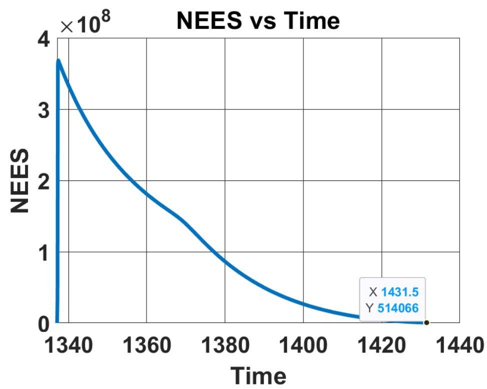


((f)) Case F

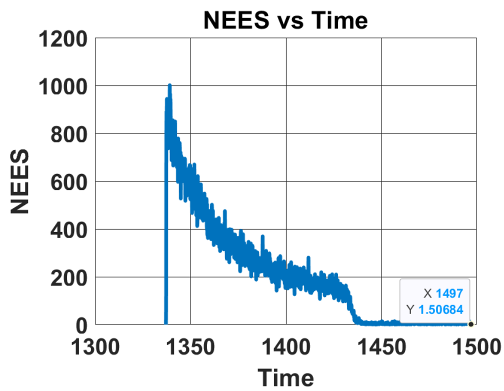


((g)) Case G

**Figure 5.5:** Cases' Comparisson - NEES vs Time

Analyzing the NEES plots reveals patterns that are distinct from the previously observed RMSE and MAE plots. Instead of observing a spike, the NEES values begin relatively low. Particularly, cases A, B, C, D, and F initiate around the $2 \times 10^4$ mark, while cases E and G start even lower, hovering near 0.5. However, this period of low values does not persist. Shortly after the initial measurements, a significant increase in NEES is evident. Case

F exhibits the most pronounced spike, leaping from a mere $1.3 \times 10^4$ to a staggering $3.7 \times 10^8$ while case E, on the other hand, sees a modest increase from 0.58 to 200.

The NEES plots can be divided into two main phases. The first phase, leading up to 1435 $s$, witnesses a characteristic and steady exponential decrease in values. This decrease, while consistent, becomes less pronounced with time, gradually reducing the rate at which NEES diminishes. It is worth noting that this behavior is unique to the NEES plots and was not observed in the RMSE and MAE plots.

Upon reaching 1435 $s$, cases E and G, the only ones to surpass this time point, display a sharp drop in NEES values. Subsequent to this drop, these cases settle into a stable plateau with values oscillating between 0.4 and 22. This plateau indicates a period of relative stability and minimal fluctuation in the Extended Kalman Filter's prediction errors. For the cases that do not proceed beyond 1435 $s$, the NEES values remain considerably high. By the end of their respective detections, cases A, B, C, D, and F converge to a value proximate to $5.15 \times 10^4$.

Consistent with the RMSE and MAE plots, the NEES data is uniformly sampled across all cases.

# 6

# Conclusions

The rapid advancements in missile technology, combined with escalating geopolitical tensions, have underscored the importance of an efficient BMDS. The study set out to evaluate the radar system in Pampilhosa da Serra for its suitability, together with an EKF algorythm, in a BMDS framework. A radar system, intended for utilization in BMDS, faces challenges in reliably tracking fast-moving missiles and algorithms that are integral to these systems, while indispensable, come with inherent complexities.

The urgency to find reliable solutions in missile tracking stems not just from a defense perspective but also from the goal of maintaining peace and preventing large-scale conflicts. An efficient BMDS acts as a deterrent, signaling the ability to neutralize threats, contributing to global security. For nations, a robust missile defense system is not just about national security, it is about international stability. Portugal's role as a NATO member, coupled with its strategic location, makes it imperative to have a system that can counter potential missile threats.

Algorithms integral to the radar system demand substantial computational power, especially when processing data in real time. Their intricate nature can introduce delays in vital decisions, affecting missile defense effectiveness. The challenge is compounded with potential biases in these algorithms, especially if they are based on incomplete or incorrect data. Adversaries' countermeasures, like decoys, further complicate the radar's task, making missile tracking even more challenging.

The objective of this thesis was to explore the suitability of the radar system located in Pampilhosa da Serra and assess how an EKF would perform for BMDS applications. Through rigorous simulations spanning various cases, insights into the system's current capabilities and potential areas of improvement were gathered. This thesis has proposed enhanced calibration methods, represented by various cases that modify radar specifications. Implementing such modifications can significantly enhance the radar system's reliability.

## 6.1 Detailed Results

The EKF, with its proven track record in estimation, was employed to gauge the performance of the radar system. While Case A provided a baseline, subsequent cases (B through G) introduced variations in the radar's specifications, simulating potential enhancements that could be made. The initial metrics from Case A were less than ideal. With an RMSE of 700 meters, MAE of 369 meters, and a NEES of $5.13695 \times 10^5$, the need for improvement was evident.

RMSE is a measure of the differences between the predicted values by the model (in this case, the radar system) and the actual values. It gives an idea of how spread out these residuals or errors are. In essence, a lower RMSE indicates a better fit to the data. An RMSE of 700 meters implies that, on average, the radar's predictions have a typical error magnitude of 700 meters. In a BMDS scenario, this is a substantial error. When dealing with fast-moving missiles, a misjudgment of 700 meters can make the difference between successful interception and a miss.

MAE quantifies how far the predictions are from the actual outcomes, giving a linear penalty to the errors. It essentially tells us the average magnitude of errors. An MAE of 369 meters indicates that the radar system, on average, misses the actual missile position by 369 meters. Such a margin of error can be critical when the goal is to intercept the missile accurately.

The NEES is a metric used to evaluate the accuracy of state estimators, like the EKF, in tracking systems. Specifically, it assesses how well the estimated state of a system (in this case, the position and velocity of a missile) matches the true state. A NEES value close to 1 indicates that the estimation error is consistent with the predicted uncertainty, signifying a good estimator. Conversely, values significantly above 1 suggest that the actual estimation errors are larger than what was anticipated, hinting at an underconfident estimator. On the other hand, values much below 1 indicate an overconfident estimator where the actual errors are smaller than the predicted uncertainty. a NEES of $5.13695 \times 10^5$ is extremely high. Such a value suggests that the estimation errors from the EKF are far larger than what the filter predicts, indicating that the estimator is highly underconfident. This means that the radar system's predictions about the missile's state are not just inaccurate, but they're also much more off-mark than the system expects them to be.

For a BMDS, this is a grave concern. A high NEES value not only points to inaccuracies in tracking but also highlights a fundamental problem with the system's ability to understand and quantify its own uncertainties. If a defense system cannot reliably predict a missile's trajectory or understand the magnitude of its own prediction errors, it can lead to significant vulnerabilities, like unsuccessful interceptions or, even worse, false confidence in a successful interception when one hasn't occurred.

However, as the radar specifications were adjusted in the subsequent cases, there were major improvements. Notably, Cases E and G exhibited significant enhancements, with their RMSE values dropping to a mere 41 meters and their NEES values nearing the optimal value of 1 and sometimes remaining below it.

In the context of industry standards, an RMSE value below 100 meters is considered desirable. The results from this thesis, particularly in Cases E and G, not only met but exceeded this benchmark, indicating the potential prowess of the radar system in Pampilhosa da Serra when augmented with the right specifications. Comparing the specifications of the radar system in Pampilhosa da Serra, which is represented in case A, with the specifications of the Gap Filling Tracking Radars (GFTR) [22] we get the following table 6.1

| Specifications | Pampilhosa | GFTR-2100/48 | GFTR-2100/51 | GFTR-2100/54 |
|---|---|---|---|---|
| $Range(km)$ | 1000 | 1400 | 2200 | 4000 |
| $Accuracy_{range}(m)$ | 75 | $< 0.5$ | $< 0.5$ | $< 0.5$ |
| $Accuracy_{angle}(rad)$ | 0.1 | $< 0.0001$ | $< 0.0001$ | $< 0.0001$ |
| $Accuracy_{velocity}(m/s)$ | 1000 | $< 0.1$ | $< 0.1$ | $< 0.1$ |
| $Range_{resolution}(m)$ | 1000 | 1 | 1 | 1 |
| $Velocity_{resolution}(m/s)$ | 1000 | 1 | 1 | 1 |
| $Beamwidth(deg)$ | 0.73 | 0.67 | 0.5 | 0.33 |

**Table 6.1:** Studied Cases' Variables

GFTR-2100 is one of the most advanced radars in the world, with functions and capabilities tailored to strengthen ballistic missile defense systems. The GFTR-2100 measures accurately at very long ranges, allowing the ballistic missile defense to protect much larger areas. Higher precision over greater distances means that the range of the radar will not limit the range of engaging missiles, as is the case with existing radars. The GFTR-2100 can simultaneously track and discriminate objects in the target cluster when a missile separates from the booster and the carrier splits into one or more warheads. Accurate discrimination increases the probability of hitting the warhead the first time.

## 6.2 Additional Considerations

**Elevation and Azimuth Limitations:** The radar system in Pampilhosa da Serra has specific elevation and azimuth movement constraints. Implementing these constraints and researching algorithms or techniques to optimize tracking could have been implemented, providing a more accurate simulation.

**Wave Travel Time:** Incorporating the time it takes for the radar signal to travel to the target and back could have provided a more accurate and realistic simulation. This would account for the time delay in the radar's measurements due to the finite speed of electromagnetic waves.

**Different Radar Types:** Investigating the performance of the EKF with various radar setups, including monostatic which is the type of radar at Pampilhosa da Serra, bistatic radars or phased array systems would have impacted the performance of the EKF.

**Advanced Filtering Techniques:** While the EKF is a powerful tool, there are other advanced filtering techniques like the Unscented Kalman Filter (UKF), Particle Filter, or the Interacting Multiple Model (IMM) filter that could be explored. These might offer better performance in certain scenarios or be more robust against non-linearities.

**Real-world Testing:** While simulations are invaluable, conducting tests with real radar systems, even if on a smaller scale or with non-threatening projectiles, would have provided practical insights and validation of the EKF.

## 6.3 Future Work

**Multiple Radar Systems:** Deploying several radars simultaneously could have provided a more comprehensive tracking solution. Individual radars can take their measurements, and fuse the data to provide a more accurate estimate. This approach could also facilitate triangulation techniques, enhancing the position estimation accuracy.

**Countermeasure Analysis:** In real-world scenarios, adversaries might deploy countermeasures such as chaff, decoys, or electronic jamming. Future studies could investigate how these countermeasures impact the tracking performance and develop techniques to mitigate their effects.

**Machine Learning and AI:** With the rise of machine learning and artificial intelligence, these technologies could be integrated into the radar system. Neural networks or other AI models might be trained to recognize missile trajectories, predict future positions, or even distinguish between actual missiles and decoys.

**Collaborative Systems:** With the advancement of networked systems, research could explore how data from other sensors (like infrared cameras, satellite systems, or sonar) could be integrated to enhance missile tracking.

## 6.4 Closing Thoughts

The radar system at Pampilhosa da Serra, when equipped with specific enhancements, has the potential to be a good tool in a BMDS framework. This thesis illuminated both its strengths and areas of improvement, setting the stage for further research and innovations in missile tracking and defense.

# References


[1] W. L. Melvin and J. A. Scheer, Principles of modern radar: Radar Applications. SciTech Publishing, 2013.

[2] C. K. Chui and G. Chen, Kalman filtering: with Real-Time Applications. Springer, 2017.

[3] E. Mazor, A. Averbuch, Y. Bar[U+2010]Shalom, and J. Dayan, "Interacting multiple model methods in target tracking: a survey," IEEE Transactions on Aerospace and Electronic Systems, vol. 34, no. 1, pp. 103–123, Jan. 1998, doi: 10.1109/7.640267.

[4] J. Elfring, E. Torta, and R. Van De Molengraft, "Particle Filters: A Hands-On Tutorial," Sensors, vol. 21, no. 2, p. 438, Jan. 2021, doi: 10.3390/s21020438.

[5] Y. K. Verma, "Design Challenges of Realizing An Active Radar Seeker at Ka-Band," 2017 IEEE MTT-S International Microwave and RF Conference (IMaRC), Dec. 2017, doi: 10.1109/imarc.2017.8449673.

[6] J. Bleriot and C. Boschet, "Key factors for the design of GAX000 radar, a new generation of UHF Early Warning Radar," 2019 International Radar Conference (RADAR), Sep. 2019, doi: 10.1109/radar41533.2019.171309.

[7] X. Wang, W. Qin, Y. Bai, and N. Cui, "Trajectory estimation for ballistic missile in boost stage using robust filtering," Iet Radar Sonar and Navigation, vol. 11, no. 3, pp. 513–519, Jan. 2017, doi: 10.1049/iet-rsn.2016.0335.

[8] K. Moon, H. Kwon, C.-K. Ryoo, and H. S. Sim, "Trajectory Estimation for a Ballistic Missile in Ballistic Phase using IR Images," 2018 9th International Conference on Mechanical and Aerospace Engineering (ICMAE), Jul. 2018, doi: 10.1109/icmae.2018.8467635.

[9] M. Asad et al., "A split target detection and tracking algorithm for ballistic missile tracking during the re-entry phase," Defence Technology, vol. 16, no. 6, pp. 1142–1150, Dec. 2020, doi: 10.1016/j.dt.2019.12.008.

[10] G. Babur, G. O. Manokhin, E. A. Monastyrev, A. A. Geltser, and A. A. A. Shibelgut, "SIMPLE CALIBRATION TECHNIQUE FOR PHASED ARRAY RADAR SYSTEMS," Progress in Electromagnetics Research M, vol. 55, pp. 109–119, Jan. 2017, doi: 10.2528/pierm16101203.

[11] D. Nguyen, B. Cho, C. Seo, J.-H. Park, and D.-H. Lee, "Analysis of the optimal frequency band for a ballistic missile defense radar system," Journal of Electromagnetic Engineering and Science, vol. 18, no. 4, pp. 231–241, Oct. 2018, doi: 10.26866/jees.2018.18.4.231.

[12] J. Kim, M. C. Lim, S.-S. Park, I. Kim, and H. Choi, "Ballistic Object Trajectory and Launch Point Estimation from Radar Measurements using Long-Short Term Memory Networks," 2019 7th International Conference on Robot Intelligence Technology and Applications (RiTA), Nov. 2019, doi: 10.1109/ritapp.2019.8932820.

[13] X. Wang, W. Qin, N. Cui, and Y. Wang, "Robust high-degree cubature information filter and its application to trajectory estimation for ballistic missile," Proceedings of the Institution of Mechanical Engineers, Part G: Journal of Aerospace Engineering, Jun. 2017, doi: 10.1177/0954410017713771.

[14] R. Cooperman, "Tactical ballistic missile tracking using the interacting multiple model algorithm," Proceedings of the Fifth International Conference on Information Fusion. FUSION 2002. (IEEE Cat.No.02EX5997), Jun. 2003, doi: 10.1109/icif.2002.1020892.

[15] H. M. T. Menegaz and S. Battistini, "Switching multiple model filter for Boost-Phase missile tracking," IEEE Transactions on Aerospace and Electronic Systems, vol. 54, no. 5, pp. 2547–2553, Oct. 2018, doi: 10.1109/taes.2018.2822118.

[16] R. Ji, Y. Liang, L. Xu, and Z. Wei, "Trajectory prediction of ballistic missiles using Gaussian process error model," Chinese Journal of Aeronautics, vol. 35, no. 1, pp. 458–469, Jan. 2022, doi: 10.1016/j.cja.2021.05.011.

[17] M. S. Grewal and A. P. Andrews, Kalman filtering: Theory and Practice Using MATLAB. Wiley-Interscience, 2001.

[18] R. L. McCoy, Modern exterior ballistics: The Launch and Flight Dynamics of Symmetric Projectiles. Schiffer Military History, 2012.

[19] G. Joos and I. M. Freeman, Theoretical Physics. Courier Corporation, 1986.

[20] W. Menke and D. Abbott, Geophysical theory. 1990.

[21] B. F. Edwards and J. Edwards, "Forces and conservation laws for motion on our spheroidal Earth," American Journal of Physics, vol. 89, no. 9, pp. 830–842, Sep. 2021, doi: 10.1119/10.0004801.

[22] "Ground-based Ballistic Missile Defense - Long-range radar," Weibel - Doppler Radars. https://weibelradars.com/explore-ballistic-missile-defense/ground/ground/ (accessed Oct. 31, 2023).

[23] B. R. Mahafza, Radar systems analysis and design using MATLAB. CRC Press, 2016.

[24] R. G. Hutchins, "Ballistic missile tracking using the interacting multiple model joint probabilistic data association filter," Sep. 01, 2013. https://calhoun.nps.edu/handle/10945/37618

[25] B. R. Mahafza and A. Elsherbeni, MATLAB simulations for radar systems design. Chapman and Hall/CRC, 2003.

[26] W. Chen, The electrical engineering handbook. 2005. [Online]. Available: http://ci.nii.ac.jp/ncid/BA70407695

[27] L. Qi, J. Guang-Long, and C. Tong, "A New Algorithm of Tracking Ballistic Missiles," Proceedings of the 2013 the International Conference on Education Technology and Information System (ICETIS 2013), Jan. 2013, doi: 10.2991/icetis-13.2013.5.

[28] M. A. Richards, J. Scheer, and W. A. Holm, Principles of modern radar. IET, 2010.

[29] W. L. Melvin and J. A. Scheer, Principles of modern radar: Advanced Techniques, Volume 2. IET, 2012.

# A

# Code of Project

**Listing A.1:** BMDRadarEKF.m

```
clear all, close all,  clc;

rho_100=[1.23E-03 1.11E-03 1.00E-03 8.97E-04 8.04E-04 7.22E-04 6.50E-04 ...
5.84E-04 5.22E-04 4.63E-04 4.07E-04 3.54E-04 3.05E-04 2.62E-04 2.24E-04 ...
1.92E-04 1.65E-04 1.41E-04 1.21E-04 1.04E-04 8.87E-05 7.58E-05 6.46E-05 ...
5.50E-05 4.69E-05 3.99E-05 3.40E-05 3.40E-05 2.46E-05 2.10E-05 1.78E-05 ...
1.52E-05 1.29E-05 1.10E-05 9.33E-06 7.95E-06 6.79E-06 5.81E-06 4.98E-06 ...
4.27E-06 3.67E-06 3.16E-06 2.73E-06 2.36E-06 2.04E-06 1.77E-06 1.55E-06 ...
1.35E-06 1.18E-06 1.04E-06 9.11E-07 8.02E-07 7.05E-07 6.21E-07 5.47E-07 ...
4.82E-07 4.24E-07 3.73E-07 3.28E-07 2.88E-07 2.88E-07 2.22E-07 1.95E-07 ...
1.71E-07 1.50E-07 1.31E-07 1.15E-07 1.00E-07 8.73E-08 7.60E-08 6.61E-08 ...
5.73E-08 4.95E-08 4.27E-08 3.68E-08 3.17E-08 2.72E-08 2.34E-08 2.00E-08 ...
1.70E-08 1.44E-08 1.21E-08 1.01E-08 8.45E-09 7.04E-09 5.89E-09 4.95E-09 ...
```

```
4.18E-09 3.56E-09 3.05E-09 2.62E-09 2.25E-09 1.94E-09 1.68E-09 1.44E-09 ...
1.24E-09 1.06E-09 9.09E-10 7.74E-10 6.55E-10 5.52E-10]*1000; %[kg/m^3]
rho_karman=[8.48E-11 1.76E-11 6.45E-12 3.15E-12 1.79E-12 1.11E-12 7.37E-13 ...
5.09E-13 3.63E-13 2.65E-13 1.97E-13 1.49E-13 1.14E-13 8.85E-14 6.92E-14 ...
5.45E-14 4.33E-14 3.46E-14 2.79E-14 2.25E-14 1.83E-14 1.49E-14 1.22E-14 ...
1.01E-14 8.32E-15 6.89E-15 5.72E-15 4.77E-15 3.98E-15 3.33E-15 2.79E-15 ...
2.35E-15 1.98E-15 1.67E-15 1.41E-15 1.19E-15 1.01E-15 8.59E-16 7.30E-16 ...
6.22E-16 5.31E-16 4.54E-16 3.88E-16 3.33E-16 2.86E-16 2.46E-16 2.12E-16 ...
1.83E-16 1.58E-16 1.37E-16 1.19E-16 1.04E-16 9.07E-17 7.94E-17 6.97E-17 ...
6.13E-17 5.41E-17 4.79E-17 4.26E-17 3.79E-17 3.39E-17 3.04E-17 2.74E-17 ...
2.47E-17 2.24E-17 2.04E-17 1.86E-17 1.71E-17 1.57E-17 1.45E-17 1.34E-17 ...
1.24E-17 1.15E-17 1.08E-17 1.01E-17 9.45E-18 8.89E-18 8.37E-18 7.91E-18 ...
7.48E-18 7.09E-18 6.74E-18 6.41E-18 6.10E-18 5.82E-18 5.56E-18 5.31E-18 ...
5.09E-18 4.87E-18 4.67E-18]*1000; %[kg/m^3]

% User-defined angles, speed and other values.
v0 = 7000;  % [m/s]
phi = 300;  % Azimuth Angle
theta = 45;  % Elevation Angle

% Position, decimal degrees
Lat = 40.105784;    %Latitude
Lon = 127.066978;   %Longitude
% Radar Position. These values need to ve close to the impact point
x_radar = 7.5553e+06+100;  % x-coordinate of radar [m]
y_radar = 8.1047e+06-100;  % y-coordinate of radar [m]
z_radar = 0;     % z-coordinate of radar [m] (since it's on the XY plane)

% System loss factor (assumed value)
L = 1.3;

% Radar Cross Section for LGM-30 Minuteman III (assumed)
sigma = 10; % [m^2]

% Radar Parameters
f_transmission = 5.56e9; % Transmission Frequency [Hz]
c = 3e8; % Speed of Light [m/s]
lambda = c / f_transmission; % Wavelength [m]
```

```
G_antenna = 10^(46/10); % Antenna Gain [linear scale]
P_peak = 5e3; % Peak Power [W]

% Range Parameters
Range_min = 50e3; % Minimum Range [m]
Range_max = 1000e3; % Maximum Range [m]
BW_receiver = 80e6; % Receiver Bandwidth [Hz]
noise_floor = -94.26; % Noise Floor [dBm]

% Missile characteristics
d = 1.85;  % Diameter [m]
A = pi * (d/2)^2;  % Cross-sectional area [m^2]
Cd = 0.15;  % Drag coefficient
m = 362;  % Mass [kg], arbitrary value

% Initial conditions
x = 4274030.934;  % [m]
y = 14512235.624;  % [m]
z = 170000;  % [m]
vx = v0 * cosd(theta) * cosd(phi);  % [m/s]
vy = v0 * cosd(theta) * sind(phi);  % [m/s]
vz = v0 * sind(theta);  % [m/s]

% Earth's rotation parameters
omega_earth = 2*pi/(24*60*60);  % [rad/s], Earth's angular velocity

% Compute gravity based on height(z)
g = 9.80665 * (6371000/(6371000 + z))^2;  % with 6371000 m Earth radius

% Time settings
dt = 0.1;  % Time step [s]
t = 0;  % Initial time [s]

% Arrays to store trajectory, speed data, range data and noisy measurements
x_data = [];
y_data = [];
z_data = [];
vx_data = [];
```

```
vy_data = [];
vz_data = [];
t_data = [];
range_data = [];
x_est_data = [];
y_est_data = [];
z_est_data = [];
X_DATA=zeros(6,14972);

i=1;
j=1;
start_detect=1;
% Loop until the missile hits the ground
while z >=10
    % Append data to arrays
    x_data = [x_data, x];
    y_data = [y_data, y];
    z_data = [z_data, z];
    vx_data = [vx_data, vx];
    vy_data = [vy_data, vy];
    vz_data = [vz_data, vz];
    t_data = [t_data, t];
    X_DATA(:,j)=[x;y;z;vx;vy;vz];


    % Air density
    if z<=100000
        rho = rho_100(floor(z/1000+1));
    else, if z>100000 && z<=1000000 && floor(z/1000)<190
            rho = rho_karman(floor(z/1000+1)-100);
    else, if z> 1000000
            rho = 0;
    else
            rho = rho_karman(1);
          end
          end
    end

```

```
    % Compute drag force and drag acceleration
    v = sqrt(vx^2 + vy^2 + vz^2);
    Fd = 0.5 * Cd * rho * v^2 * A;
    ax_d = -Fd * vx / (m * v);
    ay_d = -Fd * vy / (m * v);
    az_d = -Fd * vz / (m * v);

    % Compute coriolis acceleration
    vc = [vx; vy; vz];
    omega = [0; omega_earth*cos(Lat); omega_earth*sin(Lat)];
    a_c = 2 * cross(vc, omega);

    %Compute Eotvos acceleration
    ae_z = vx * omega_earth * cosd(Lat);

    %Compute the SUM of accelerations
    a = [ax_d + a_c(1);
         ay_d + a_c(2);
         az_d + a_c(3) - g + ae_z];

    % Update velocities considering drag and gravity
    vx = vx + a(1) * dt;
    vy = vy + a(2) * dt;
    vz = vz + a(3) * dt;

    % Calculate distance from radar to missile
    dx = x - x_radar;
    dy = y - y_radar;
    dz = z - z_radar;

    % Calculate true range and azimuth
    range_true = sqrt(dx^2 + dy^2 + dz^2);
    azimuth_true = atan2(dy, dx);
    elevation_true = asin(dz/range_true);

    if range_true >= Range_min && range_true <= Range_max
        % Calculate received power using radar equation (simplified version)
        Pr = (P_peak * G_antenna^2 * lambda^2 * sigma) ./ ...
```

```
    ((4*pi)^3 * range_true.^4 * L);
    Pr_dBm = 10*log10(Pr/1e-3); % Convert received power to dBm

    % Check if received power is above noise floor
    if Pr_dBm > noise_floor
        if i==1
            %start_detect variable used for later RMSE and MAE calculations
            start_detect=size(t_data,2);
            x0 = [x + randn * 1333; y + randn * 1333; z + randn * 1333; ...
            vx+ randn * 16.6667; vy+ randn * 16.6667; vz+ randn * 16.6667];
            P = diag([4000^2, 4000^2, 4000^2, 50^2, 50^2, 50^2]);
            Q = diag([100^2, 100^2, 100^2, 10^2, 10^2, 10^2]);
            R = diag([75^2, (0.2*pi/180)^2, (0.05*pi/180)^2]);
            X_est = [];
            P_estimated = {};
            X_est(:, 1) = x0;
            P_est = P;
            P_estimated{1}=P_est;
            x_est_data = [x_est_data, X_est(1,i)];
            y_est_data = [y_est_data, X_est(2,i)];
            z_est_data = [z_est_data, X_est(3,i)];
            range_data = [range_data, range_true];

            i=i+1;
            F = [1 0 0 dt 0 0;
                 0 1 0 0 dt 0;
                 0 0 1 0 0 dt;
                 0 0 0 1 0 0;
                 0 0 0 0 1 0;
                 0 0 0 0 0 1];
        end

        % Convert true coordinates to polar and generate noisy measurements
        %(assuming noise is Gaussian)
        range_scaling_factor = (Range_max - range_true) / ...
        (Range_max - Range_min);

        range_error = 75 * range_scaling_factor;
```

```
        azimuth_error = (0.2 * pi / 180) * range_scaling_factor;
        elevation_error = (0.05 * pi / 180) * range_scaling_factor;

        measured_Range = range_true + range_error * randn;
        measured_phi = azimuth_true + azimuth_error * randn;
        measured_theta = elevation_true + elevation_error * randn;

        X_pred = F * X_est(:, i-1);

        % x = x0 + vx0*dt + 1/2*a(1)*dt^2
        X_pred(1) = X_pred(1) + 0.5*a(1)*dt^2;
        % y = y0 + vy0*dt + 1/2*a(2)*dt^2
        X_pred(2) = X_pred(2) + 0.5*a(2)*dt^2;
        % z = z0 + vz0*dt + 1/2*(az_d - g)*dt^2
        X_pred(3) = X_pred(3) + 0.5*a(3)*dt^2;

        % vx = vx + a(1) * dt;
        X_pred(4) = X_pred(4) + a(1) * dt;
        % vy = vy + a(2) * dt;
        X_pred(5) = X_pred(5) + a(2) * dt;
        % vz = vz + (az_d - g) * dt;
        X_pred(6) = X_pred(6) + a(3) * dt;

        P_pred = F * P_est * F' + Q;

        dx_pred = X_pred(1) - x_radar;
        dy_pred = X_pred(2) - y_radar;
        dz_pred = X_pred(3) - z_radar;

        % Update Step
        h = [sqrt(dx_pred^2 + dy_pred^2 + dz_pred^2);
             atan2(dy_pred, dx_pred);
             asin(dz_pred/sqrt(dx_pred^2 + dy_pred^2 + dz_pred^2))];


        H_j = [dx_pred/h(1), dy_pred/h(1), dz_pred/h(1), 0, 0, 0;
               -dy_pred/(dx_pred^2 + dy_pred^2), dx_pred/(dx_pred^2 + ...
               dy_pred^2), 0, 0, 0, 0;
```

```
                   -dx_pred*dz_pred/(sqrt(-dz_pred^2/(dx_pred^2 + ...
                   dy_pred^2 + dz_pred^2) + 1)*(dx_pred^2 + dy_pred^2 +...
                   dz_pred^2)^(3/2)), -dy_pred*dz_pred/(sqrt(-dz_pred^2/...
                   (dx_pred^2 + dy_pred^2 + dz_pred^2) + 1)*(dx_pred^2 + ...
                   dy_pred^2 + dz_pred^2)^(3/2)), (-dz_pred*dz_pred/ ...
                   (dx_pred^2 + dy_pred^2 + dz_pred^2)^(3/2) + ...
                   1/sqrt(dx_pred^2 + dy_pred^2 + dz_pred^2))/...
                   sqrt(-dz_pred^2/(dx_pred^2 + dy_pred^2 + dz_pred^2) + 1)...
                   , 0, 0, 0];


            K = P_pred * H_j' / (H_j * P_pred * H_j' + R);
            X_est(:, i) = X_pred + K * ([measured_Range; measured_phi; ...
            measured_theta] - h);
            P_est = (eye(6) - K * H_j) * P_pred;
            P_estimated{i}=P_est;

            R = diag([range_error^2, azimuth_error^2, elevation_error^2]);

            x_est_data = [x_est_data, X_est(1,i)];
            y_est_data = [y_est_data, X_est(2,i)];
            z_est_data = [z_est_data, X_est(3,i)];
            range_data = [range_data, range_true];
            i=i+1;
        end
    end

    % Updates
    x = x + vx * dt + a(1) * dt^2;
    y = y + vy * dt + a(2) * dt^2;
    z = z + vz * dt + a(3) * dt^2;
    g = 9.80665 * (6371000/(6371000 + z))^2;  % with 6371000 m Earth radius
    t = t + dt;
    j=j+1;
end

% Append data to arrays
x_data = [x_data, x];
```

```
y_data = [y_data, y];
z_data = [z_data, z];
vx_data = [vx_data, vx];
vy_data = [vy_data, vy];
vz_data = [vz_data, vz];
t_data = [t_data, t];
X_DATA(:,j)=[x;y;z;vx;vy;vz];

%end_detect variable used for later RMSE and MAE calculations
end_detect=length(range_data);
impactPoint = [x,y,z]

% Plotting the trajectory in 3D
figure;
plot3(x_data, y_data, z_data, 'b', ...
x_est_data, y_est_data, z_est_data, 'r', 'Linewidth', 3);
xlabel('X (m)');
ylabel('Y (m)');
zlabel('Altitude (Z) (m)');
title('Missile Trajectory');
grid on;

% Plotting the speed vs time
figure;
plot(t_data, vx_data,'r', t_data, vy_data,'g', ...
t_data, vz_data, 'b', 'Linewidth', 3);
xlabel('Time (s)');
ylabel('Velocity (m/s)');
title('Missile Speed vs Time');
legend('Vx', 'Vy', 'Vz');
grid on;

v_data = sqrt(vx_data.^2 + vy_data.^2 + vz_data.^2);
figure;
plot(t_data, v_data, 'k', 'Linewidth', 3);
xlabel('Time (s)');
ylabel('Velocity Magnitude (m/s)');
title('Velocity Magnitude vs Time');
```

```
grid on;

% Other statistics
disp(['Maximum Altitude Achieved: ', num2str(max(z_data)), ' m']);
disp(['Maximum Speed Achieved: ', num2str(max(v_data)), ' m/s']);
disp(['Total Flight Time: ', num2str(t), ' s']);
disp(['Ground Distance travelled: ', num2str(sqrt(x^2+y^2)), ' m']);
```

**Listing A.2:** RmseMaeEkf.m

```
%RMSE, MAE
% If the code is giving an error it's probably because the radar isn't
% detecting the missile, consider changing the position of the radar with
% help of the impact point.
RMSEx=rmse(x_data(:,start_detect:start_detect+end_detect-1),x_est_data);
RMSEy=rmse(y_data(:,start_detect:start_detect+end_detect-1),y_est_data);
RMSEz=rmse(z_data(:,start_detect:start_detect+end_detect-1),z_est_data);
disp(['RMSE X: ', num2str(RMSEx), ' m']);
disp(['RMSE Y: ', num2str(RMSEy), ' m']);
disp(['RMSE Z: ', num2str(RMSEz), ' m']);
disp(['Overall RMSE: ', num2str(sqrt(RMSEx^2+RMSEy^2+RMSEz^2)), ' m']);
disp(' ');
MAEx=mae(x_data(:,start_detect:start_detect+end_detect-1),x_est_data);
MAEy=mae(y_data(:,start_detect:start_detect+end_detect-1),y_est_data);
MAEz=mae(z_data(:,start_detect:start_detect+end_detect-1),z_est_data);
disp(['MAE X: ', num2str(MAEx), ' m']);
disp(['MAE Y: ', num2str(MAEy), ' m']);
disp(['MAE Z: ', num2str(MAEz), ' m']);
disp(['Overall MAE: ', num2str((MAEx+MAEy+MAEz)/3), ' m']);
disp(' ');

rmse_valuesA = zeros(length(range_data), 1);
mae_valuesA = zeros(length(range_data), 1);
rmse_valuesB = zeros(length(range_data), 1);
mae_valuesB = zeros(length(range_data), 1);
time_values = zeros(length(range_data), 1);
range_values = zeros(length(range_data), 1);
nees_values = zeros(length(range_data),1);
```

```
for i = 0:length(x_est_data)-1
    start_idx = start_detect;
    end_idx = start_detect+end_detect-1+i;

    % Calculate RMSE and MAE
    rmse_valuesA(i+1) = sqrt(rmse(x_data(:,start_detect:start_detect+i),...
    x_est_data(:,1:1+i))^2 + rmse(y_data(:,start_detect:start_detect+i),...
    y_est_data(:,1:1+i))^2 + rmse(z_data(:,start_detect:start_detect+i),...
    z_est_data(:,1:1+i))^2);

    mae_valuesA(i+1) = (mae(x_data(:,start_detect:start_detect+i),...
    x_est_data(:,1:1+i)) + mae(y_data(:,start_detect:start_detect+i),...
    y_est_data(:,1:1+i)) + mae(z_data(:,start_detect:start_detect+i),...
    z_est_data(:,1:1+i))) / 3;

    rmse_valuesB(i+1) = sqrt(rmse(x_data(:,start_detect+i:start_detect+i),...
    x_est_data(:,1+i:1+i))^2 + rmse(y_data(:,start_detect+i:start_detect+i),...
    y_est_data(:,1+i:1+i))^2 + rmse(z_data(:,start_detect+i:start_detect+i),...
    z_est_data(:,1+i:1+i))^2);

    mae_valuesB(i+1) = (mae(x_data(:,start_detect+i:start_detect+i),...
    x_est_data(:,1+i:1+i)) + mae(y_data(:,start_detect+i:start_detect+i),...
    y_est_data(:,1+i:1+i)) + mae(z_data(:,start_detect+i:start_detect+i),...
    z_est_data(:,1+i:1+i))) / 3;

end
for i = 1:length(range_data)
    true_state = X_DATA(:, length(X_DATA)-length(range_data)+i);
    estimated_state = X_est(:, i);
    P_current = cell2mat(P_estimated(i));
    error = true_state - estimated_state;
    nees_values(i) = error' * inv(P_current) * error;
end

% Plotting the results. Cumulative RMSE and MAE
figure;
subplot(2,2,1);
```

```
plot(t_data(:,start_detect:start_detect+end_detect-1), rmse_valuesA);
xlabel('Time');
ylabel('RMSE');
title('RMSE vs Time');

subplot(2,2,2);
plot(t_data(:,start_detect:start_detect+end_detect-1), mae_valuesA);
xlabel('Time');
ylabel('MAE');
title('MAE vs Time');

subplot(2,2,3);
plot(range_data, rmse_valuesA);
xlabel('Range');
ylabel('RMSE');
title('RMSE vs Range');

subplot(2,2,4);
plot(range_data, mae_valuesA);
xlabel('Range');
ylabel('MAE');
title('MAE vs Range');



% Plotting the results. Descretized RMSE and MAE
figure;
subplot(2,2,1);
plot(t_data(:,start_detect:start_detect+end_detect-1), rmse_valuesB);
xlabel('Time');
ylabel('RMSE');
title('RMSE vs Time');

subplot(2,2,2);
plot(t_data(:,start_detect:start_detect+end_detect-1), mae_valuesB);
xlabel('Time');
ylabel('MAE');
title('MAE vs Time');
```

```
subplot(2,2,3);
plot(range_data, rmse_valuesB);
xlabel('Range');
ylabel('RMSE');
title('RMSE vs Range');

subplot(2,2,4);
plot(range_data, mae_valuesB);
xlabel('Range');
ylabel('MAE');
title('MAE vs Range');

%NEES values
figure;
plot(t_data(:,start_detect:start_detect+end_detect-1), nees_values);
xlabel('Time');
ylabel('NEES');
title('NEES vs Time');
```